AN ABSTRACT OF THE THESIS OF

Bethany Ruth Robinson for the degree of Master of Science in Nuclear Engineering presented on June 8, 2011.
Title: Investigation of a Hybrid Quasi-diffusion/Monte Carlo Method for Solving Multigroup Criticality Problems in Slab Geometry

Abstract approved: _____

Todd S. Palmer

A hybrid Quasi-diffusion/Monte Carlo Method for solving multigroup criticality problems in slab geometry was investigated. Analog Monte Carlo was used to calculate functionals (Eddington Factors) that were then used in solution of the quasi-diffusion equations. The hybrid method was shown to accurately and precisely predict the k-eigenvalue and fission source distribution for loosely coupled problems with high dominance ratios and significant spatial gradients. The hybrid method was also shown to be computationally more efficient than analog Monte Carlo.

©Copyright by Bethany R. Robinson

June 8, 2011

All Rights Reserved

Investigation of a Hybrid Quasi-diffusion/Monte Carlo Method for Solving Multigroup Criticality Problems in Slab Geometry

by

Bethany R. Robinson

A THESIS

submitted to

Oregon State University

in partial fulfillment of
the requirements for the
degree of

Master of Science

Presented June 8, 2011
Commencement June 2012

Master of Science thesis of Bethany R. Robinson presented on June 8, 2011.

APPROVED:

Major Professor, representing Nuclear Engineering

Head of the Department of Nuclear Engineering and Radiation Health Physics

---

Dean of the Graduate School

I understand that my thesis will become part of the permanent collection of Oregon State University libraries. My signature below authorizes release of my thesis to any reader upon request.

Bethany R. Robinson, Author

ACKNOWLEDGEMENTS

I would like to thank Dr. Todd Palmer for his help and support in my thesis work. This thesis work is based on his ideas and could not have been done without his help. I would also like to thank him for his help in my graduate class work. He is an excellent instructor and was always willing to set time aside to help me in his classes and with concepts I was struggling with in classes taught by other professors.

I would like to thank my committee members; Dr. Steve Binney, Dr. Ken Krane, and Dr. Henri Jansen for there time and commitment to my thesis work. Without their approval and feedback this thesis would not have been possible. I would also like to thank them for working with me to set up my defense in a short time frame. I would specifically like to thank Dr. Steve Binney for praying for me and encouraging me throughout my graduate work.

I would like to thank my family for their support during my academic studies. I would like to thank my dad for encouraging me to take my love for mathematics and apply it to Nuclear Engineering. Without his encouragement I would not be where I am today. I would like to thank my brothers, Joshua and Matthew. They are amazing study partners. I would like to thank my brother Noah for his encouragement and help with learning the C++ programming language. I would like to thank my brother Zachary, sister Arynne, and sister-in-law Fama for just being who they are. And a special thanks to my nephews and niece Joseph, Jonathan, Daniel, and Lydia for the joy they have brought into my life throughout my graduate work.

I would like to thank my fellow students. I would especially like to thank Matt

Cleveland for his help with C++ programming.

I would like to thank my friends. I have been blessed with some amazing friends who have prayed for me and encouraged me along the way. Specifically I would like to thank Laurie Binney who has been like a 2nd mother to me. Her prayers and encouragement have been a precious gift.

Most importantly I would like to thank my Lord and Savior Jesus Christ. How amazing it is to not only be a adopted, through Jesus death and resurrection into God's family, but to have the King of the universe walking with me and helping me every moment of my life. He is the reason that I live.

TABLE OF CONTENTS

TABLE OF CONTENTS (Continued)

LIST OF FIGURES

LIST OF FIGURES (Continued)

LIST OF FIGURES (Continued)

LIST OF FIGURES (Continued)

LIST OF FIGURES (Continued)

LIST OF TABLES

LIST OF TABLES (Continued)

Investigation of a Hybrid Quasi-Diffusion/Monte Carlo Method for Solving Multigroup Criticality Problems in Slab Geometry

1 Introduction

There is increasing interest in "hybrid methods" for the purpose of accelerating the convergence of the fission source and eigenvalue in k-eigenvalue radiation transport problems. Hybrid methods are methods that make use of two or more methods for solving radiation transport problems. In the past there have been two general approaches in the field of numerical radiation transport: Monte Carlo methods and deterministic methods. Currently, however, there is more and more interest in combining the two methods to form hybrid methods in the hopes of making use of the more desirable qualities of each, while minimizing the disadvantages.

The equation that governs radiation transport is an integro-differential equation that can be solved analytically only for very simple problems, but can be solved numerically for more complex problems. In deterministic methods the transport equation is converted into a system of algebraic equations by discretizing each of the independent variables in the equation. Common numerical methods used for discretizing the angular variable include S_N methods and P_N methods. In S_N methods the angular dependence of the flux is represented by a discrete set of directions (or rays) whereas in the P_N method, functional expansions are used to discretize the angular variables [Dud. 1976]. Another commonly used method is Monte Carlo. Monte Carlo makes use of pseudo-random numbers to track individual histories through a system that are representative of particles of radiation.

For systems which are mostly governed by diffusion, for example commercial nuclear reactors, diffusion theory is commonly used. However, diffusion theory

assumes weak angular dependence and breaks down near boundaries or where material properties change dramatically over distances comparable to a mean free path. Diffusion theory is also inaccurate near localized sources and in strongly absorbing media. Generally diffusion theory is valid in weakly absorbing media several mean free paths from any sources or boundaries.

Another method which will also be discussed extensively in this thesis is quasi-diffusion which was first proposed as a deterministic method by Gol'din in 1964 [Gol. 1964]. It was later implemented successfully by Miften and Larsen with newly-derived boundary conditions in 1993 [Mif. 1993].

The hybrid method discussed in this thesis makes use of quasi-diffusion in conjunction with standard analog Monte Carlo. The objective is to accelerate the convergence of the fission source in Monte Carlo k-eigenvalue calculations where the fissionable components are loosely-coupled and fission source convergence is extremely slow. For this type of problem, the complications go beyond the slow convergence of the fission source. Because of the statistics involved in Monte Carlo calculations and the loose coupling between components of these problems, unphysical spatial gradients in the initial fission source may never be damped out or may be amplified. The hybrid method proposed in this thesis is specifically geared toward criticality problems with high dominance ratios that are very challenging for standard Monte Carlo methods.

1.1 Literature Review

1.1.1 Analog Monte Carlo

Monte Carlo for the solution of complex problems was made possible by the invention of the first electronic computer in 1945. In fact it was only two years after the invention of the first electronic computer that John von Neumann outlined a letter to Robert Richtmyer, the Theoretical Division leader at Los Alamos, regarding a possible statistical approach to solving the problem of neutron diffusion in fissionable material [Met. 1987].

John von Neumann's interest in random numbers was triggered by discussions with Stan Ulam whose extensive mathematical background made him aware that with the development of the electronic computer statistical sampling techniques were now possible. Before the development of the electronic computer the performance of such calculations had ceased to be considered because the tediousness of the calculations and length of time required was too great an impediment [Met. 1987].

However it is reported that John von Neumann was not the first to use Monte Carlo in the study of neutron behavior. According to Emilio Segre, a student and collaborator of Enrico Fermi, nearly 15 years earlier Fermi had used statistical methods when he was studying the moderation of neutrons in Rome. He did not publish anything on the subject, but used the method to solve many problems with a small mechanical adding machine. After the invention of the first electronic computer, which was called the ENIAC, Fermi had an instrument built, later called the FERMIAC, which developed neutron genealogies in two dimensions and was able to accommodate two neutron energies, slow and fast [Met. 1987].

Monte Carlo was the name suggested by N. Metropolis for the statistical method and was inspired by Stan Ulam's uncle who would borrow money from relatives

because he "just had to go to Monte Carlo." [Met. 1987]

Analog Monte Carlo, also called direct simulation, can be thought of in much the same way as an analog circuit where the input is proportional to the output. For example, a radiation particle entering with a weight of one will never have a weight greater than one. It will either remain alive with a weight of one or be absorbed and die. In a shielding problem, using analog Monte Carlo, a particle that is tallied at the other side of the shield actually made its way through the shield without being absorbed. This is quite different than with non analog Monte Carlo. With implicit Monte Carlo particles often change weight as they move through material and tallies are often based on fractions of the original particle. Implicit Monte Carlo is used to solve thermal radiative transfer problems. Many variance reduction techniques make use of implicit Monte Carlo including: absorption suppression, splitting and Russian roulette, weight windows, and many others [Lew. 1993].

Monte Carlo methods have spread rapidly and today are used extensively in the study of radiation transport. They are used in the nuclear and medical physics industries for a large range of problems including criticality, reactor calculations, shielding, and dose. The Monte Carlo N-Particle Transport Code, MCNP, available from the Radiation Safety Information Computational Center, RSICC, [MCNP 2009], is the most commonly used Monte Carlo code for radiation transport calculations.

1.1.2 Quasi Diffusion

Quasi-diffusion was first introduced into the area of deterministic methods in 1964 by Gol'din [Gol. 1964]. Troshchiev et al. was the first to report results from quasi-diffusion's use as a true acceleration scheme [Tro. 1968], obtaining the same

solutions from the acceleration scheme as the unaccelerated transport equations. In 1979, Aksenov and Gol'din applied the quasi-diffusion method to the two-dimensional stationary equation of neutron transport and showed that the quasi-diffusion method retains its efficiency for two-dimensional problems [Aks. 1979].

A Fourier stability analysis of Goldin's [Gol. 1964] quasi-diffusion method for iteratively solving discrete-ordinates problems was performed in 1990 by Cefus and Larsen. They showed that the method was stable and rapidly converging for all mesh sizes [Cef. 1990].

In 1993, Anistratov and Gol'din [Ani. 1993] published their work on nonlinear methods for solving particle transport problems, which they called Quasi Projective (QP) methods. The quasi-diffusion method and nonlinear flux methods (both first and second flux methods) were considered with both consistent and independent differencing schemes.

In 2005 Hiruta, Anistratov, and Adams published work on a splitting method for solving the coarse-mesh discretized low-order quasi-diffusion equations [Hik. 2005]. This methodology was developed for reactor physics calculations and was shown to effectively split a problem into two parts: a tensor diffusion problem that captures a significant part of the transport solution in the central part of an assembly, and a calculation for the complicated behavior of the transport solution near assembly boundaries [Hik. 2005]. Also in 2005, Anistratov published his work on consistent spatial approximation of the low-order quasi-diffusion equations on coarse grids [Ani. 2005]. Anistratov's proposed homogenization procedure reproduced accurately the complicated large-scale behavior of the transport solution within assemblies.

Miften and Larsen derived new boundary conditions for quasi-diffusion and

successfully implemented them in 1993 [Mif. 1993]. Two years later, Urbatsch used these boundary conditions in his development of a hybrid Monte Carlo/quasi-diffusion method in his PhD thesis work [Urb. 1995]. His hybrid method was the basis for the research presented in this thesis. The method shown in this thesis differs from Urbatsch's work in the order and number of iterations between the quasi-diffusion and the Monte Carlo in an attempt to do more of the work in the lower order and less computationally expensive solver. This thesis also extends the method to multiple energy groups, whereas Urbatsch's work focused on the energy-independent transport equation. In addition, Wiedlandt acceleration was used to accelerate the convergence of the quasi-diffusion solve in the one-group eigenvalue problems.

1.1.3 Hybrid Methods

Hybrid methods for radiation transport make use of two or more methods for solving radiation transport problems. The hybrid method in this thesis makes use of both quasi-diffusion and analog Monte Carlo techniques. Monte Carlo is used to calculate functionals (Eddington factors) that are then used in the solution of the quasi-diffusion equations.

Other hybrid methods have been developed making use of quasi-diffusion for problems with high dominance ratios. Larsen and Yang published their work in 2007 on Monte Carlo Functional methods for estimation of k-eigenvalues and eigenfunctions [Lar. 2007]. In 2008 Larsen and Yang applied their work on Monte Carlo Functional Methods to the solution of k-eigenvalue problems [Lar. 2008].

In addition to criticality problems, hybrid methods have been and are being developed for source detection and shielding problems. In the early-mid 1990's

a commercial British code MCBEND was released. In MCBEND a Monte Carlo module was merged with a diffusion module to calculate weight windows. In the late 1990's LANL developed the AVATAR package. The AVATAR package made use of a discrete-ordinates code to generate direction-dependent weight windows for MCNP. Although the AVATAR package no longer exists, in recent years ORNL has released the CADIS package which provides automated software links between an existing discrete-ordinates code and an existing Monte Carlo code. CADIS has the advantage that the user only has to write one input deck and the code does all the rest.

In 2003 Haghighat and Wagner published a review on Monte Carlo variance reduction with deterministic importance functions [Hag. 2003]. In addition to other researchers work, Haghighat and Wagner's publication reviews their own methodology which is used in the CADIS package. In 2005 Smith and Wagner did a study on manual and automated Monte Carlo variance reduction with a deep penetration reactor shielding problem [Smi. 2005]. Their work is applicable to the analysis of reactor problems where reactor transients cause a reduction in moderator temperature, increasing the attenuation of neutrons and decreasing the response of excore detectors.

1.2 Thesis Overview

The remainder of this thesis is organized as follows:

I. Derivation of Mono-Energetic Quasi-Diffusion in Slab Geometry

II. Discretization of the Mono-Energetic Quasi-Diffusion Equation in Slab Geometry

2 Methods

2.1 Introduction

The purpose behind the hybrid Monte Carlo method discussed in this chapter is to accelerate the convergence of the fission source in Monte Carlo k-eigenvalue calculations where the fissionable components are loosely-coupled. In addition to the complications caused by the slow convergence of the fission source, the statistics involved in Monte Carlo calculations and the loose coupling between components of these problems may cause unphysical spatial gradients in the initial fission source to persist or be amplified. The less "communication" between regions, the greater the possibility of this situation. It is even possible in problems where a region is neutronically isolated from its neighbors, that all the particles could end up in one region.

The hybrid method makes us of an iteration scheme between Monte Carlo transport and a quasi-diffusion low order (QDLO) equation. The majority of the work is done in the QDLO solver which makes use of functionals (Eddington factors) obtained from the Monte Carlo code. This decreases computational time since one iteration in the QDLO code can be much less expensive than one iteration in the transport Monte Carlo code.

This method is based on the quasi-diffusion method, first proposed by Gol'din [Gol. 1964] in 1964 with boundary conditions derived by Miften and Larsen in 1993 [Mif. 1993].

We begin with the derivation and discretization of the quasi-diffusion equations in slab geometry, followed by a discussion of the analog Monte Carlo method used

to obtain the Eddington factors. The iteration method used in this work will then be discussed.

2.2 Derivation of Mono-energetic Quasi-Diffusion in Slab Geometry

The mono-energetic, one-dimensional integro-differential transport equation for a slab of width L with vacuum boundaries is shown below, where ψ represents the angular flux, Σ_t, Σ_s, and Σ_f are the total, scattering, and fission cross sections, respectively, ν is the number of neutrons produced per fission, k is the multiplication faction (k-eigenvalue), and μ is component of the neutron's direction vector along the x-axis.

$$\mu\frac{\partial\psi(x,\mu)}{\partial x} + \Sigma_t(x)\psi(x,\mu) = \frac{1}{2}(\Sigma_s(x) + \frac{\nu\Sigma_f(x)}{k})\int \psi(x,\mu)\,d\mu, \tag{1}$$

$$\psi(0,\mu) = 0, \quad \mu > 0, \tag{2}$$

$$\psi(L,\mu) = 0, \quad \mu < 0, \tag{3}$$

The angular moment of the angular flux ψ, is defined in Equation 4, where ϕ_0 is the scalar flux.

$$\phi_n(x) = \int_{-1}^{1} \mu^n\psi(x,\mu)\,d\mu, \tag{4}$$

The transport equation, Eq. (1), integrated over angle is shown below in Equation 5.

$$\frac{d\phi_1(x)}{dx} + \Sigma_t(x)\phi_0(x) = (\Sigma_s(x) + \frac{\nu\Sigma_f(x)}{k})\phi_0(x) \tag{5}$$

The transport equation is multiplied by μ and integrated over angle to obtain a relationship between $\phi_1(x)$ and $\phi_2(x)$ as shown in Equation 6.

$$\frac{d\phi_2(x)}{dx} + \Sigma_t(x)\phi_1(x) = 0 \tag{6}$$

Equation 6 is then solved for $\phi_1(x)$ to yield:

$$\phi_1(x) = -\frac{1}{\Sigma_t(x)}\frac{d\phi_2(x)}{dx} \tag{7}$$

Substituting Equation 7 into Equation 5 yields:

$$-\frac{d}{dx}\frac{1}{\Sigma_t(x)}\frac{d}{dx}\phi_2(x) + \Sigma_a(x)\phi_0(x) = \frac{\nu\Sigma_f(x)}{k}\phi_0(x) \tag{8}$$

No approximation to the transport equation has been made at this point.

A definition for an "Eddington factor"', λ_2 is shown in Equation 9.

$$\lambda_2(x) \equiv \frac{\phi_2(x)}{\phi_0(x)} = \frac{\int_{-1}^{1}\mu^2\psi(x,\mu)\,d\mu}{\int_{-1}^{1}\psi(x,\mu)\,d\mu} \tag{9}$$

The first term in Equation 8 is then multiplied and divided by $\phi_0(x)$ while the remaining terms are multiplied and divided by λ_2 to obtain the elliptic equation for $\lambda_2(x)\phi_0(x)$ shown in Equation 10.

$$-\frac{d}{dx}\frac{1}{\Sigma_t(x)}\frac{d}{dx}\lambda_2(x)\phi_2(x) + \frac{\Sigma_a(x)}{\lambda_2(x)}\lambda_2(x)\phi_0(x) = \frac{\nu\Sigma_f(x)}{k\lambda_2(x)}\lambda_2(x)\phi_0(x) \tag{10}$$

2.2.1 Vacuum Boundary Conditions

The vacuum boundary conditions at $x = 0$ and $x = L$, as derived by Miften and Larsen, are obtained by integrating Equation 2 over $\mu > 0$:

$$\begin{aligned} 0 &= \int_0^1 \mu\psi(0,\mu)\,d\mu - \int_{-1}^0 \mu\psi(0,\mu)\,d\mu + \int_0^1 \mu\psi(0,\mu)\,d\mu + \int_{-1}^0 \mu\psi(0,\mu)\,d\mu, \\ &= \int_0^1 |\mu|\psi(0,\mu)\,d\mu + \int_{-1}^0 |\mu|\psi(0,\mu)\,d\mu + \int_0^1 \mu\psi(0,\mu)\,d\mu + \int_{-1}^0 \mu\psi(0,\mu)\,d\mu, \\ &= \int_{-1}^1 |\mu|\psi(0,\mu)\,d\mu + \int_{-1}^1 \mu\psi(0,\mu)\,d\mu. \end{aligned} \tag{11}$$

The integration and manipulation for the right hand boundary condition is shown below.

$$\begin{aligned} 0 &= \int_{-1}^{0} \mu\psi(L,\mu)\,d\mu - \int_{0}^{1} \mu\psi(L,\mu)\,d\mu + \int_{-1}^{0} \mu\psi(L,\mu)\,d\mu + \int_{0}^{1} \mu\psi(L,\mu)\,d\mu, \\ &= -\int_{-1}^{0} |\mu|\psi(L,\mu)\,d\mu - \int_{0}^{1} |\mu|\psi(L,\mu)\,d\mu + \int_{-1}^{0} \mu\psi(L,\mu)\,d\mu + \int_{0}^{1} \mu\psi(L,\mu)\,d\mu, \\ &= -\int_{-1}^{1} |\mu|\psi(L,\mu)\,d\mu + \int_{-1}^{1} \mu\psi(L,\mu)\,d\mu. \end{aligned} \tag{12}$$

The Eddington factors for the boundaries are defined in Equations 13 and 14 and are essentially a ratio of the total current and flux at the surface.

$$\lambda_1(0) = \left(\frac{\int_{-1}^{1} |\mu|\psi(0,\mu)\,d\mu}{\int_{-1}^{1} \psi(0,\mu)\,d\mu} \right) \tag{13}$$

$$\lambda_1(L) = \left(\frac{\int_{-1}^{1} |\mu|\psi(L,\mu)\,d\mu}{\int_{-1}^{1} \psi(L,\mu)\,d\mu} \right) \tag{14}$$

Equation 7 at $x = 0$ and $x = L$ is then rewritten by multiplying and dividing the right hand side by $\phi_0(0)$ and $\phi_0(L)$ and substituting in Equation 9 to obtain:

$$\phi_1(0) = -\frac{1}{\Sigma_t(x)} \frac{d}{dx} \lambda_2(0)\phi_0(0), \tag{15}$$

$$\phi_1(L) = -\frac{1}{\Sigma_t(x)} \frac{d}{dx} \lambda_2(L)\phi_0(L). \tag{16}$$

The last term in Equations 11 and 12 are $\phi_1(0)$ and $\phi_1(L)$ respectively. Substituting Equations 13 and 15 into Equation 11 and Equations 14 and 16 into Equation 12, the left and right vacuum boundary conditions become

$$0 = \lambda_1(0)\phi_0(0) - \frac{1}{\Sigma_t(0)} \frac{d}{dx} \lambda_2(0)\phi_0(0), \tag{17}$$

$$0 = \lambda_1(L)\phi_0(L) + \frac{1}{\Sigma_t(L)}\frac{d}{dx}\lambda_2(L)\phi_0(L). \tag{18}$$

Multiplying both sides by $\lambda_2(0)/\lambda_1(0)$ and $\lambda_2(L)/\lambda_1(L)$ the left and right boundary conditions can be written as shown in Equations 19 and 20.

$$0 = \lambda_2(0)\phi_0(0) - \frac{\lambda_2(0)}{\lambda_1(0)\Sigma_t(0)}\frac{d}{dx}\lambda_2(0)\phi_0(0) \tag{19}$$

$$0 = \lambda_2(L)\phi_0(L) + \frac{\lambda_2(L)}{\lambda_1(L)\Sigma_t(L)}\frac{d}{dx}\lambda_2(L)\phi_0(L) \tag{20}$$

Equations 10, 19, and 20 constitute the QDLO equations used in this thesis, derived without approximation from the transport problem described by Equations 1, 2, and 3.

2.2.2 Reflecting Boundary Conditions

With reflecting boundaries, the net flow through the surface is zero, such that

$$J(0) = 0, \tag{21}$$

$$J(L) = 0. \tag{22}$$

Recalling the definitions for current in Equations 15 and 16, the reflecting boundary conditions can also be written as shown below:

$$0 = -\frac{1}{\Sigma_t(x)}\frac{d}{dx}\lambda_2(0)\phi_0(0), \tag{23}$$

$$0 = -\frac{1}{\Sigma_t(x)}\frac{d}{dx}\lambda_2(L)\phi_0(L). \tag{24}$$

2.3 Discretization of the Mono-Energetic Quasi-Diffusion Equation in Slab Geometry

The QDLO equations were discretized in space using a standard finite volume method. We begin with the QDLO modified diffusion equation shown in Equation 25, where $\tilde{\phi}(x) = \phi_0(x)\lambda_2(x)$:

$$-\frac{d}{dx}\frac{1}{\Sigma_t(x)}\frac{d}{dx}\tilde{\phi}(x) + \frac{\Sigma_a(x)}{\lambda_2(x)}\tilde{\phi}(x) = \frac{1}{k}\frac{\nu\Sigma_f(x)}{\lambda_2(x)}\tilde{\phi}(x) \tag{25}$$

The QDLO equation is discretized by integrating over a cell width from $x_{i-\frac{1}{2}}$ to $x_{i+\frac{1}{2}}$ as shown in Equation 26.

$$-\int_{x_{i-\frac{1}{2}}}^{x_{i+\frac{1}{2}}}\left[\frac{d}{dx}\frac{1}{\Sigma_t(x)}\frac{d}{dx}\tilde{\phi}(x)\right]dx + \int_{x_{i-\frac{1}{2}}}^{x_{i+\frac{1}{2}}}\frac{\Sigma_a(x)}{\lambda_2(x)}\tilde{\phi}(x)\,dx = \int_{x_{i-\frac{1}{2}}}^{x_{i+\frac{1}{2}}}\frac{\nu\Sigma_f(x)}{k\lambda_2(x)}\tilde{\phi}(x)\,dx \tag{26}$$

Integrating and substituting in the definition of current, J (Equation 27) into Equation 26 yields

$$J(x) = \phi_1(x) = -\frac{1}{\Sigma_t(x)}\frac{d\tilde{\phi}}{dx} \tag{27}$$

$$J(x_{i+\frac{1}{2}}) - J(x_{i-\frac{1}{2}}) + \frac{\Sigma_{a,i}}{\lambda_{2,i}}\tilde{\phi}_i\Delta x_i = \frac{1}{k}\frac{\nu\Sigma_{f,i}}{\lambda_{2,i}}\tilde{\phi}_i\Delta x_i. \tag{28}$$

The surface current, $J_{i+\frac{1}{2}}$ is defined by Equations 29 and Equation 30 where D is like a modified diffusion coefficient and is equal to $\frac{1}{\Sigma_t}$.

$$J_{i+\frac{1}{2}} = J(x_{i+\frac{1}{2}}) = -\frac{D_{i+1}\left(\tilde{\phi}_{i+1} - \tilde{\phi}_{i+\frac{1}{2}}\right)}{\frac{\Delta x_{i+1}}{2}}, \tag{29}$$

$$J_{i+\frac{1}{2}} = J(x_{i+\frac{1}{2}}) = -\frac{D_i\left(\tilde{\phi}_{i+\frac{1}{2}} - \tilde{\phi}_i\right)}{\frac{\Delta x_i}{2}}. \tag{30}$$

Equations 29 and 30 are set equal to each other and solved for $\tilde{\phi}_{i+\frac{1}{2}}$ to obtain

$$\tilde{\phi}_{i+\frac{1}{2}} = \frac{D_{i+1}\tilde{\phi}_{i+1}\Delta x_i + D_i\tilde{\phi}_i\Delta x_{i+1}}{D_{i+1}\Delta x_i + D_i\Delta x_{i+1}}. \tag{31}$$

Equation 31 is then inserted into Equation 29 to obtain an expression for $J_{i+\frac{1}{2}}$ in terms of known quantities.

$$J_{i+\frac{1}{2}} = \left[-\frac{2D_iD_{i+1}}{D_{i+1}\Delta x_i + D_i\Delta x_{i+1}}\right]\tilde{\phi}_{i+1} + \left[\frac{2D_iD_{i+1}}{D_{i+1}\Delta x_i + D_i\Delta x_{i+1}}\right]\tilde{\phi}_i. \tag{32}$$

A similar expression for $J_{i-\frac{1}{2}}$ is shown below

$$J_{i-\frac{1}{2}} = \left[-\frac{2D_iD_{i-1}}{D_i\Delta x_{i-1} + D_{i-1}\Delta x_i}\right]\tilde{\phi}_i + \left[\frac{2D_iD_{i-1}}{D_i\Delta x_{i-1} + D_{i-1}\Delta x_i}\right]\tilde{\phi}_{i-1}. \tag{33}$$

Equations 32 and 33 are inserted into Equation 28 to obtain

$$\begin{aligned}
&-\left[\frac{2D_iD_{i-1}}{D_i\Delta x_{i-1} + D_{i-1}\Delta x_i}\right]\tilde{\phi}_{i-1} \\
&+\left[\frac{2D_{i+1}D_i}{D_{i+1}\Delta x_i + D_i\Delta x_{i+1}} + \frac{2D_iD_{i-1}}{D_i\Delta x_{i-1} + D_{i-1}\Delta x_i} + \frac{\Sigma_{a,i}\Delta x_i}{\lambda_{2,i}}\right]\tilde{\phi}_i \\
&-\left[\frac{2D_{i+1}D_i}{D_{i+1}\Delta x_i + D_i\Delta x_{i+1}}\right]\tilde{\phi}_{i+1} = \frac{1}{k}\frac{\nu\Sigma_{f,i}\Delta x_i}{\lambda_{2,i}}\tilde{\phi}_i.
\end{aligned} \tag{34}$$

2.3.1 Discretization of Vacuum Boundary Conditions

Recalling the definition for current in Equation 27 and inserting into Equations 19 and 20 yields

$$\tilde{\phi}(0) = -\frac{\lambda_{2,0}}{\lambda_{1,0}}J(0), \tag{35}$$

$$\tilde{\phi}(L) = \frac{\lambda_{2,L}}{\lambda_{1,L}}J(L). \tag{36}$$

The volume discretized definitions for $J(0)$ and $J(L)$ as defined in Equation 30 and shown below in Equations 37 and 38 where $J_{i-\frac{1}{2}} = J(0)$ and $J_{i+\frac{1}{2}} = J(L)$.

$$J(0) = -\frac{D_1(\tilde{\phi}_1 - \tilde{\phi}(0))}{\frac{\Delta x_1}{2}} \tag{37}$$

$$J(L) = -\frac{D_I(\tilde{\phi}(L) - \tilde{\phi}_I)}{\frac{\Delta x_I}{2}} \tag{38}$$

Equations 37 and 38 are inserted into 35 and 36 and solved for $\tilde{\phi}(0)$ and $\tilde{\phi}(L)$ to find

$$\tilde{\phi}(0) = \frac{2\lambda_{2,0}D_1}{\lambda_{1,0}\Delta x_1 + 2\lambda_{2,0}D_1}\tilde{\phi}_1, \tag{39}$$

$$\tilde{\phi}(L) = \frac{2\lambda_{2,L}D_I}{\lambda_{1,L}\Delta x_I + 2\lambda_{2,L}D_I}\tilde{\phi}_I. \tag{40}$$

Using the definitions for $\tilde{\phi}(0)$ and $\tilde{\phi}(L)$ in the the boundary conditions for $J(0)$ and $J(L)$ gives an expression for the boundary current in terms of cell-average fluxes:

$$J(0) = -\frac{2\lambda_{1,0}D_1\tilde{\phi}_1}{\lambda_{1,0}\Delta x_1 + 2\lambda_{2,0}D_1}, \tag{41}$$

$$J(L) = \frac{2\lambda_{1,L}D_I\tilde{\phi}_I}{\lambda_{1,L}\Delta x_I + 2\lambda_{2,L}D_I}. \tag{42}$$

These last two equations are inserted into Equation 28 to obtain discretized equations for the left and right boundaries

$$\left[\frac{2D_2D_1}{D_2\Delta x_1 + D_1\Delta x_2} + \frac{2D_1\lambda_{1,0}}{\lambda_{1,0}\Delta x_1 + 2\lambda_{2,0}D_1} + \frac{\Sigma_{a,1}\Delta x_1}{\lambda_{2,1}}\right]\tilde{\phi}_1$$

$$-\left[\frac{2D_2D_1}{D_2\Delta x_1 + D_1\Delta x_2}\right]\tilde{\phi}_2 = \frac{1}{k}\frac{\nu\Sigma_{f,1}\Delta x_1}{\lambda_{2,1}}\tilde{\phi}_1; \tag{43}$$

$$-\left[\frac{2D_ID_{I-1}}{D_I\Delta x_{I-1} + D_{I-1}\Delta x_I}\right]\tilde{\phi}_{I-1}$$

$$+\left[\frac{2D_ID_{I-1}}{D_I\Delta x_{I-1} + D_{I-1}\Delta x_I} + \frac{2D_I\lambda_{1,L}}{\lambda_{1,L}\Delta x_I + 2\lambda_{2,L}D_I} + \frac{\Sigma_{a,I}\Delta x_I}{\lambda_{2,I}}\right]\tilde{\phi}_I +$$

$$= \frac{1}{k}\frac{\nu\Sigma_{f,I}\Delta x_I}{\lambda_{2,I}}\tilde{\phi}_I \tag{44}$$

Equations 34, 43, and 44 have the form of a tri-diagonal matrix and can be solved for cell average $\tilde{\phi}$ values using a standard tri-diagonal matrix solver.

2.3.2 Discretization of Reflecting Boundary Conditions

Inserting $J_{I-\frac{1}{2}} = J(0) = 0$, and/or $J_{\frac{1}{2}} = J(0) = 0$ into Equation 28 yields

$$\left[\frac{2D_2D_1}{D_2\Delta x_1 + D_1\Delta x_2} + \frac{\Sigma_{a,1}\Delta x_1}{\lambda_{2,1}}\right]\tilde{\phi}_1 - \left[\frac{}{D_2\Delta x_1 + D_1\Delta x_2}\right]\tilde{\phi}_2$$

$$= \frac{1}{k}\frac{\nu\Sigma_{f,1}\Delta x_1}{\lambda_{2,1}}\tilde{\phi}_1 \tag{45}$$

$$-\left[\frac{2D_ID_{I-1}}{D_I\Delta x_{I-1} + D_{I-1}\Delta x_I}\right]\tilde{\phi}_{I-1} + \left[\frac{2D_ID_{I-1}}{D_I\Delta x_{I-1} + D_{I-1}\Delta x_I} + \frac{\Sigma_{aI}\Delta x_I}{\lambda_{2I}}\right]\tilde{\phi}_I$$

$$= \frac{1}{k}\frac{\nu\Sigma_{fI}\Delta x_I}{\lambda_{2I}}\tilde{\phi}_I \tag{46}$$

.

2.4 Derivation of One-Dimensional Quasi-Diffusion with Multiple Energy Groups in Slab Geometry

The energy-dependent, one-dimensional integro-differential transport equation for a slab of width L with vacuum boundaries is described in Equations 47, 48, and 49.

$$\mu\frac{\partial\psi(x,\mu,E)}{\partial x} + \Sigma_t(x,E)\psi(x,\mu,E) = \frac{1}{2}\int\Sigma_s(x,E'\rightarrow E)\psi(x,\mu,E')dE'd\mu$$

$$+\frac{\chi(x,E)}{2k}\int\nu\Sigma_f(x,E')\psi(x,\mu',E')dE'd\mu', \tag{47}$$

$$\psi(0,\mu,E) = 0, \quad \mu > 0, \tag{48}$$

$$\psi(L,\mu,E) = 0, \quad \mu < 0. \tag{49}$$

The angular moment of the angular flux ϕ is defined in Equation 50, where ϕ_0 is the scalar flux.

$$\phi_n(x) = \int_{-1}^{1}\mu^n\psi(x,\mu,E)\,d\mu, \tag{50}$$

Integrating 47 over angle gives Equation 51.

$$\frac{\partial\phi_1(x,E)}{\partial x}+\Sigma_t(x,E)\phi_0(x,E)=\int\Sigma_s(x,E'\rightarrow E)\phi_0(x,E')dE'$$

$$+\frac{\chi(x,E)}{k}\int\nu\Sigma_f(x,E')\phi_0(x,E')dE'. \tag{51}$$

The transport equation, Equation 47, is multiplied by μ and integrated over angle to obtain a relationship between $\phi_1(x,E)$ and $\phi_2(x,E)$:

$$\frac{d\phi_2(x,E)}{dx}+\Sigma_t(x,E)\phi_1(x,E)=0. \tag{52}$$

Equation 52 was solved for $\phi_1(x,E)$ and is shown below in Equation 53.

$$\phi_1(x,E)=-\frac{1}{\Sigma_t(x,E)}\frac{d\phi_2(x,E)}{dx} \tag{53}$$

Substituting the relationship between $\phi_1(x,E)$ and $\phi_2(x,E)$ into Equation 51 yields

$$-\frac{d}{dx}\frac{1}{\Sigma_t(x,E)}\frac{d}{dx}\phi_2(x,E)+\Sigma_t(x,E)\phi_0(x,E)=\int\Sigma_s(x,E'\rightarrow E)\phi_0(x,E')dE'$$

$$+\frac{\chi(x,E)}{k}\int\nu\Sigma_f(x,E')\phi_0(x,E')dE', \tag{54}$$

with no approximation.

A definition for an "Eddington factor", $\lambda_2(x,E)$, is shown in Equation 55.

$$\lambda_2(x,E)\equiv\frac{\phi_2(x,E)}{\phi_0(x,E)}=\frac{\int_{-1}^{1}\mu^2\psi(x,\mu,E)\,d\mu}{\int_{-1}^{1}\psi(x,\mu,E)\,d\mu}. \tag{55}$$

The first term in Equation 54 is multiplied and divided by $\phi_0(x,E)$ while the remaining terms are multiplied and divided by $\lambda_2(x,E)$ to obtain the elliptic equation

for $\lambda_2(x,E)\phi_0(x,E)$ shown in Equation 56.

$$-\frac{d}{dx}\frac{1}{\Sigma_t(x,E)}\frac{d}{dx}\lambda_2(x,E)\phi_0(x,E)+\frac{\Sigma_t(x,E)}{\lambda_2(x,E)}\lambda_2(x,E)\phi_0(x,E)$$

$$=\int\frac{\Sigma_s(x,E'\rightarrow E)\lambda_2(x,E')\phi_0(x,E')}{\lambda_2(x,E')}dE'$$

$$+\frac{\chi(E,x)}{k}\int\frac{\nu\Sigma_f(x,E')}{\lambda_2(x,E')}\lambda_2(x,E')\phi_0(x,E')dE' \tag{56}$$

Defining $\lambda_2(x,E)\phi_0(x,E)$ as $\tilde{\phi}_0(x,E)$ gives Equation 57.

$$-\frac{d}{dx}\frac{1}{\Sigma_t(x,E)}\frac{d}{dx}\tilde{\phi}_0(x,E)+\frac{\Sigma_t(x,E)}{\lambda_2(x,E)}\tilde{\phi}_0(x,E)$$

$$=\int\frac{\Sigma_s(x,E'\rightarrow E)\tilde{\phi}_0(x,E')}{\lambda_2(x,E')}dE'$$

$$+\frac{\chi(x,E)}{k}\int\frac{\nu\Sigma_f(x,E')}{\lambda_2(x,E')}\tilde{\phi}_0(x,E')dE' \tag{57}$$

The boundary conditions were developed in the same manner for the energy-dependent equation as they were for the mono-energetic equation and the same process was used to develop the discretized equations.

2.5 Monte Carlo Transport

Monte Carlo transport methods are used extensively in the nuclear physics field. Monte Carlo methods are based on physical probabilities and make use of repeated sampling of random or pseudo-random numbers. The equation that governs the transport of radiation is an integro-differential equation that is not easy to solve analytically without approximation. While Monte Carlo is especially nice for solving neutron transport problems, it has some major limitations. The main limitation with Monte Carlo methods is the computational time necessary to obtain a solution for many problems. Theoretically, if an infinite number of histories are run, a

perfect solution without approximation can be obtained. However, since the error decreases with the square root of the number of histories it can take a very large number of histories to obtain a suitable answer. This is the reason that much research is focused on coupling deterministic methods with Monte Carlo Methods.

Monte Carlo transport is also exceedingly easy to understand and implement. Basically, particles (histories) of radiation are created and followed through their life to determine physical parameters.

In this section, the focus is on the development of the probabilistic interpretation of neutron transport used to calculate the fission source and Eddington factors used in the hybrid method discussed in this thesis. Much of this material is found in *Computational Methods of Neutron Transport* [Lew. 1993].

In Monte Carlo, each individual neutron undergoes a random process that is governed by simple statistical laws. For example, a neutron born into a problem can either be absorbed, fission (a type of absorption), scatter, or leak out of the problem. Each of these events has a certain probability of occurrence based on the cross sections of the background material. If the problem has reflecting boundaries, absorption and scattering are the only options.

Every material has scattering, capture, and fission cross sections. These cross sections are dependent on the material and the energy of the radiation interacting with the material. The total cross section is the sum of all the material cross sections. There are two ways of defining cross sections: microscopic and macroscopic.

Microscopic cross-sections characterize the probability of a neutron interaction with an individual nucleus. It can be defined as the effective area per single nucleus for a given interaction. The units for microscopic cross-sections are $\frac{interaction-cm^2}{neutron-nucleus}$. Because the size of the nucleus is so small, microscopic cross-sections are often

measured in units of *barns* (b), where a *barn* is equal to $10^{-24} cm^2$.

Macroscopic cross sections characterize the probability of neutron interaction in a chunk of material (the target) and can be defined as the probability per unit length that a neutron will undergo a particular type of interaction. Macroscopic cross sections have units of $\frac{interactions}{neutron-cm}$ and are equal to the atom density of the material multiplied by its microscopic cross section.

2.5.1 Probabilistic Interpretation of Events

Consider a one-group, isotropically-scattering slab, $0 < x < L\,cm$, with vacuum boundaries. A random neutron born anywhere in this slab has three possible outcomes; absorption in the slab or leakage out of the left or right edge. Suppose we wish to calculate the probability that a random neutron will leak out the left edge or right edge, respectively; P_L and P_R, and the probability that the neutron will be absorbed somewhere in the slab, P_{AB}. Since these are the three only possible outcomes it is also true that $P_L + P_R + P_{AB} = 1$.

The sampling method used in Monte Carlo is based on pseudo random numbers, between 0 and 1. As an example consider $A_1, A_2, A_3, ..., A_n$ to be independent mutually exclusive events with probabilities $p_1, p_2, p_3, ..., p_n$, respectively. Since they are mutually exclusive, $p_1 + p_2 + p_3 + ... + p_n = 1$ and p_1 can be thought of as a subinterval of the unit interval from 0 to 1. If a random number, ξ, where $(0 \leq \xi \leq 1)$, lies in the interval $p_1 + ... + p_{i-1} \leq \xi < p_1 + ... + p_i$ then ξ determines event A_i.

For a given sampling for the example considered above a sequence of random numbers $\xi_k (k = 1, 2, 3, ..n)$ is generated, and if ξ_k is an element of subinterval n_k where $(1 \leq n_k \leq n)$, then a sequence of events, E_{n_k}, occurs, where each event E_i

occurs with probability p_i.

The *probability density function* (PDF) can be used to derive the probabilistic interpretation of events.

$$p(x) = \{p_i \qquad i-1 \leq x < i \qquad 1 \leq i \leq n\} \tag{58}$$

A PDF of a random variable is a function which describes the density of probability at each point in the sample space. The probability of a random variable falling within a given set is given by the integral of its density over the set. A PDF is a continuous function that when integrated over all x is equal to 1.

Using the PDF, the cumulative probability distribution function (CPDF) of x is defined as the probability that x lies between 0 and X.

$$P(x) = \int_0^x p(t)\,dt \tag{59}$$

The event x can be calculated in terms of ξ by setting the CPDF equal to the random number ξ. If ξ is a random number in the interval $0 \leq \xi < 1$, then x will fall on the interval $i-1 \leq x < i$ with a probability of p_i and event E_i will occur with probability p_i

The advantage of using CPDFs to describe the probabilistic interpretation of events is that they work well for PDFs that are continuous functions of a variable. Equation 60 determines x as a function of ξ such that x lies on the interval between x and $x + dx$ with the probability $p(x)\,dx$:

$$\xi = P(x) = \int_0^x p(t)\,dt \tag{60}$$

The disadvantage of using CPDFs is that they can be used in a Monte Carlo code only if Equation 60 can be explicitly solved for x as a function of ξ. There are other methods used for those equations that cannot be solved explicitly for ξ.

2.5.2 Analog Monte Carlo Sampling

The location of birth of a neutron in a particular cell was determined from the PDF shown in Equation 61.

$$p(x) = \begin{cases} 0, & 0 \leq x < x_L, \\ \frac{1}{x_R - x_L} & x_L \leq x < x_R, \\ 0, & x_R \leq x < L. \end{cases} \tag{61}$$

where x_L and x_R are the left and right cell boundaries and L and x are the right edge of the slab and the birth place of the neutron, respectively.

The CPDF is defined in Equation 62.

$$P(x) = \int_a^x p(t)\, dt = \begin{cases} 0, & 0 \leq x < x_L, \\ \frac{x - x_L}{x_R - x_L,} & x_L \leq x < x_R, \\ 1, & x_R \leq x < L. \end{cases} \tag{62}$$

where $P(x)$ is the probability that the neutron is born between a and x. If ξ is set equal to $P(x)$ with the requirement that $0 < \xi < 1$ then $\xi = \frac{x - x_L}{x_R - x_L}$ and x can be determined from Equation 63.

$$x = x_L + (x_R - x_L)\, \xi \tag{63}$$

Assuming that a random neutron is born isotropically in its direction cosine μ, the pdf for the direction of flight is $p(\mu) = \frac{1}{2}$, where $\mu = \cos\theta$ and $-1 \leq \mu \leq 1$. The direction is then obtained by defining the CPDF as shown below in Equation 64 and setting it equal to a random number ξ where $0 < \xi < 1$.

$$P(\mu) = \xi = \int_{-1}^{\mu} \frac{1}{2}\, d\mu,$$

$$\xi = \frac{\mu + 1}{2}, \tag{64}$$

$$\mu = 2\xi - 1.$$

The probability of collision of a neutron between s and $s+ds$, where s represents the length of the path traversed by the neutron, is given by $p(s)\, ds = \Sigma_t e^{-\Sigma_t s}$,

where $\Sigma_t\, ds$ is equal to the probability of having a collision in ds and $e^{-\Sigma_t s}$ is the probability of a particle traveling a distance s without a collision. From this it can be seen that the pdf can be defined as shown in Equation 65, where $\int_0^\infty p(s)\, ds = 1$.

$$p(s) = \Sigma_t e^{-\Sigma_t s} \tag{65}$$

The CPDF is shown in Equation 66.

$$\begin{aligned} P(s) &= \int_0^s p(t)\, dt, \\ &= \int_0^s \Sigma_t e^{-\Sigma_t s}\, ds, \\ &= 1 - e^{-\Sigma_t s}. \end{aligned} \tag{66}$$

Setting the CPDF equal to a random number ξ where $0 < \xi < 1$ the distance to collision can be calculated from Equation 67.

$$s = -\frac{1}{\Sigma_t} \ln \xi \tag{67}$$

In analog Monte Carlo, once the neutron has a collision, the type of collision (scattering or absorption), can be determined from the scattering ratio which is equal to $\frac{\Sigma_s}{\Sigma_t}$. If the random number ξ is less than $\frac{\Sigma_s}{\Sigma_t}$ the event is a scattering event and if it is greater than $\frac{\Sigma_s}{\Sigma_t}$ the event is an absorption event. If the event is a scattering event a new direction of flight is sampled and the history continued and if the event is absorption the history is terminated. In those problems that deal with multiple energies, if the neutron scatters, there is an additional sampling to determine whether the neutron changes energy as a result of the scattering event.

Absorption suppression (also called survival biasing or implicit capture), is a non analog Monte Carlo method used to decrease the variance. In absorption suppression, [Lew. 1993], a particle's history is not terminated by absorption and

the criterion $\frac{\Sigma_s}{\Sigma_t}$ is no longer used to determine whether the particle will survive the event or not. Instead, all collisions are treated as scattering events, where the weight of the particle at the ith collision is reduced by the survival probability:

$$w_{n,i+1} = w_{n,i}\left(1 - \frac{\Sigma_a}{\Sigma_t}\right). \tag{68}$$

Although this procedure lengthens the computing time per history, since the number of collisions is increased, it is more than offset by the reduction in variance, providing a good criteria for history termination is used.

2.5.3 Tracking Procedures and Tallies

The tracking procedure in the slab geometry Monte Carlo solver is performed as follows. On the first generation the birth location of a neutron history is determined based on Equation 63 and an equal number of neutron histories were assigned to each cell. A random number is used to determine the direction of flight of the history as shown in Equation 64 and the distance to collision is calculated using Equation 67. If the distance to collision is greater than the distance to the cell edge, the neutron's path length, path length squared, and path length multiplied by μ^2 are tallied. The neutron is then moved to the cell edge and a new random number is used to calculate the distance to collision using Equation 67. This process is continued until the distance to collision is less than the distance to the cell edge. When this occurs the tallies mentioned above are recorded and a random number is used to determine whether the collision is a scatter or absorption event. If the event is a scattering event, a random number is used to determine, based on scattering cross-sections, what energy group the neutron had scatters to and Equation 64 is used to determine a new direction. For the mono-energetic Monte Carlo the neutron does not change energy groups. If the event is an absorption event, a

random number is used to determine whether the event is capture or fission. If the absorption event is a capture the history is terminated. If the event is a fission event the location of the event is saved before terminating the history. The fission sites are then used in the next generation to determine the birth location of the neutrons (histories). The fission distribution was used to determine how many histories to give birth to at each fission site.

Initially in this work, an attempt was made to use the cell averaged fission distribution to determine the weight of histories in each cell. An equal number of histories were started in each cell and the location of birth was determined randomly, rather than keeping track of the individual fission site locations. It was found using this averaging method that in those places where large gradients occurred, the fission distribution was not accurately preserved. In addition an attempt was made to linearize the sampling procedure in each cell (sample based on the slope of the fission distribution in each cell), but although this method performed better as would be expected, it still did not preserve the fission distribution as accurately as was desired.

The track length is tallied using the standard track length estimator shown in Equation 69.

$$x_n = \sum_i w_{n,i} l_{n,i} \tag{69}$$

where x_n is the track length in cell n, $w_{n,i}$ is the weight of particle i in cell n, and $l_{n,i}$ is equal to the length traveled by particle i in cell n.

The total track length tallied for each cell was used to calculate the cell-averaged flux in each cell using Equation 70.

$$\bar{\phi}_n = \frac{x_n}{(\Delta x_n)\,(N_{tot})} \tag{70}$$

Equation 71 was used to tally the square of the track length.

$$x_n^2 = \sum_i w_{n,i} {l_{n,i}}^2 \tag{71}$$

The sum of the the square of the track length and the sum of the track length tallies were than used to calculate the standard deviation of the track length in each cell as shown in Equation 72. The derivation of the sample standard deviation can be found in Lewis and Miller's book *Computational Methods of Neutron Transport* [Lew. 1993].

$$S = \left(\frac{N}{N-1} \right)^{1/2} \left\{ \frac{1}{N} \sum_{n=1}^{N} x_n^2 - \hat{x}^2 \right\}^{1/2} \tag{72}$$

The standard deviation of the track length is used to calculate the standard deviation of the cell averaged flux and the cell averaged fission source distribution in each cell.

The Eddington factors calculated by the Monte Carlo code for use in the quasi-diffusion part of the hybrid method are obtained as an average of the angle squared, weighted by the track length flux estimate shown in Equation 73.

$$\lambda_{2,m} = \frac{\sum_{i=1}^{N} \sum_{k(i)=1}^{K(i)} \left(\mu_i^2 \; l_i \; w_i \right)_{k(i),m}}{\sum_{i=1}^{N} \sum_{k(i)=1}^{K(i)} \left(l_i \; w_i \; \right)_{k(i),m}} \tag{73}$$

where λ_{2m} is the Eddington functional for cell m, N the total number of particles, and l_i is the track length in cell m for track $k(i)$ of particle i.

At the boundaries the Eddington factor, λ_2, is the ratio of an angle-weighted surface current estimate and a surface flux estimate [Lew. 1993] as shown for the left and right boundaries respectively in 74 and 75.

$$\lambda_2(0) = \frac{\sum_{i=1}^{N} |\mu_i(0)| \, w_i(0)}{\sum_{i=1}^{N} \left(w_i(0) / |\mu_i(0)| \right)} \tag{74}$$

$$\lambda_2(L) = \frac{\sum_{i=1}^{N} |\mu_i(L)|\, w_i(L)}{\sum_{i=1}^{N} \left(w_i(L)/\,|\mu_i(L)|\right)} \tag{75}$$

In addition to the Eddington factor at the boundaries there are also Eddington functionals at the boundaries, λ_1, which are calculated from a ratio of the particle current and a surface flux estimate at the surface as shown in Equation 76 and 77, respectively.

$$\lambda_1(0) = \frac{w_i(0)}{\Sigma_{i=1}^{N} \left(w_i(0)/\,|\mu_i(0)|\right)} \tag{76}$$

$$\lambda_1(L) = \frac{w_i(L)}{\Sigma_{i=1}^{N} \left(w_i(L)/\,|\mu_i(L)|\right)} \tag{77}$$

The variance estimates of λ_1 and λ_2 are expected to be smaller than the variances associated with the Monte Carlo estimates for flux. This is because the $\lambda' s$ are constrained between zero and one, while flux values throughout the system can differ by many orders of magnitude. In addition the statistical errors tend to cancel, since the $\lambda' s$ are ratios of similar quantities.

2.6 Implementation of the Hybrid Method

The iteration scheme for this hybrid method involves making an initial guess for the Eddington factors of 1/3, which is consistent with diffusion theory. The QDLO equation is then iterated until convergence and the resulting fission source distribution and k-eigenvalue are used as the initial guesses in the transport Monte Carlo code. Several Monte Carlo fission generations are then calculated to generate improved estimates of the Eddington factors and boundary functionals. This new data is then used in the QDLO solver along with the source distribution and k-eigenvalue from the Monte Carlo as initial guesses and the problem is iterated again until convergence. This process is continued a specified number of times.

The Eddington factors and boundary functionals are calculated from the track length in each cell as shown in Section 2.5.3.

The QDLO equations were solved using a standard finite volume discretization for cell averaged fluxes as shown in Section 2.3. Power iteration was used to calculate the k-eigenvalue and fission source distribution in the QDLO.

3 Results

3.1 Introduction

In this chapter, we describe several test problems which will be used to assess the performance of the new hybrid MC/QD in comparison with standard Monte Carlo and discrete ordinates methods. We begin with mono-energetic test problems, including a test problem formulated by Urbatsch [Urb. 1995] designed to be slowly convergent for standard Monte Carlo. We then consider several multigroup problems to demonstrate the efficacy of the low-order quasi-diffusion solver to speed convergence on the fission source. Numerical results from these problems are used to evaluate the hybrid method from the perspectives of accuracy and efficiency, and we discuss the physical reasons behind the trends we observe.

3.2 Mono-energetic Results

Results will be shown for three different problems. Problem 1 is a homogeneous problem defined by Miften and Larsen [Mif. 1993]. This problem is composed of 50 cells, each 1.0 cm across. The cross sections of the material are shown in Table 1. The boundary conditions are reflecting on the left hand side and vacuum on the right. Figure 1 shows the spatial refinement of this problem 1.

Region	Σ_t	Σ_t	$\nu\Sigma_f$
1	1.0	0.2	0.8

Table 1: Material Properties (Problem 1)

Problem 2 is a two region problem composed of 8 cm of fuel followed by 8 cm of moderator. The 16.0 cm slab is discretized into 16 equal cells, 1.0 cm in thickness.

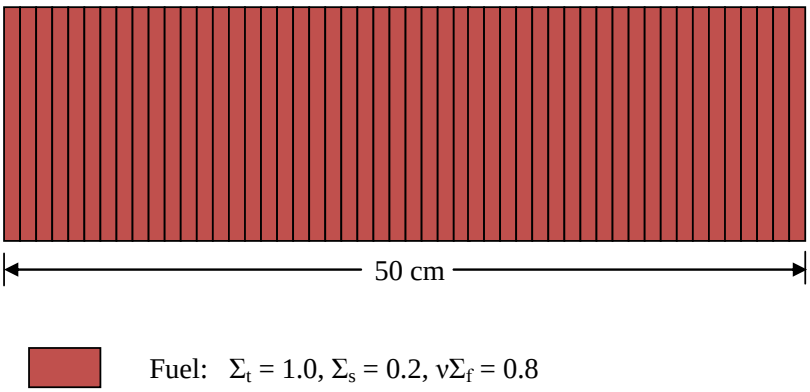

Figure 1: Problem 1

Table 2 show the material properties of the fuel and moderator. We consider two variations of this problem: reflecting boundary on the left/vacuum boundary on the right, and vacuum boundary on left/reflecting boundary on the right.

Region	Σ_t	Σ_s	$\nu\Sigma_f$
1	1.0	0.7	0.3071
2	1.0	0.001	0.0

Table 2: Material Properties (Problem 2)

Problem 3 is a heterogeneous problem defined by Urbatsch [Urb. 1995]. This problem has 39 regions of alternating fuel and moderator materials. Region one is 1.0 cm of moderator discretized into 8 equal length cells, followed by a region of fuel 2.0 cm in length and discretized into 16 equal length cells. The fuel is followed by another 1.0 cm region of moderator and another 2.0 cm region of fuel. This pattern continues for all 39 regions, ending with a 1.0 cm region of moderator. The cross-sections of fuel and moderator are the same as those of Problem 2. Both the left and right hand boundaries are vacuum. A pictorial representation of Problem 3 is shown in Figure 3 and 4 below.

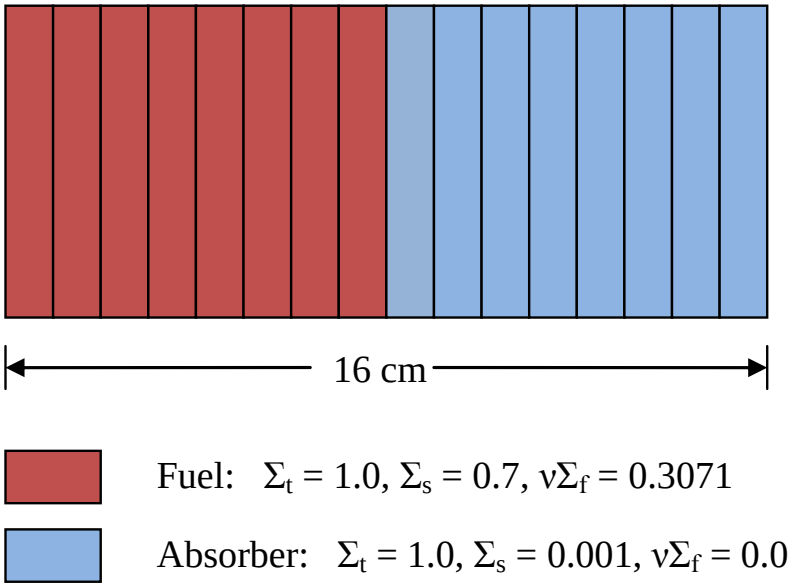

Figure 2: Problem 2

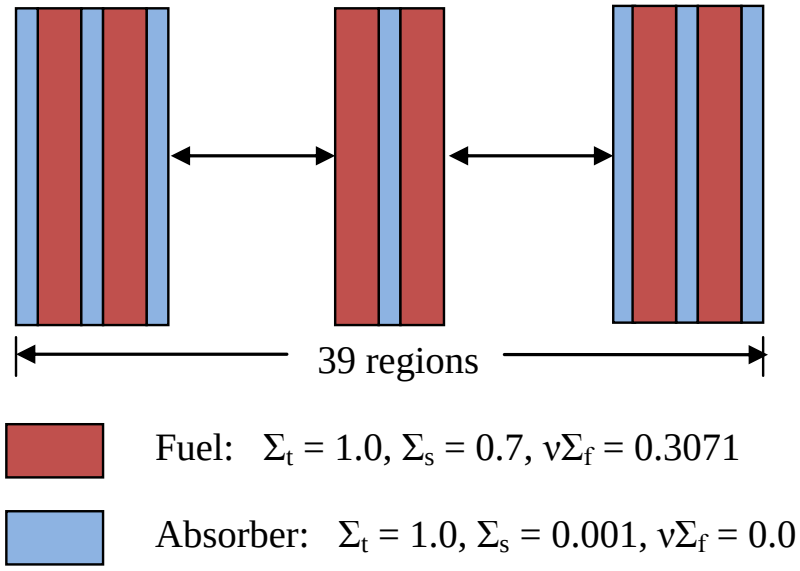

Figure 3: Problem 3

3.2.1 Test Problem #1

Problem 1 was solved using 50,000, 500,000 and 5,000,000 histories per MC generation. In each case, the fission source distribution, multiplication factor and slowest

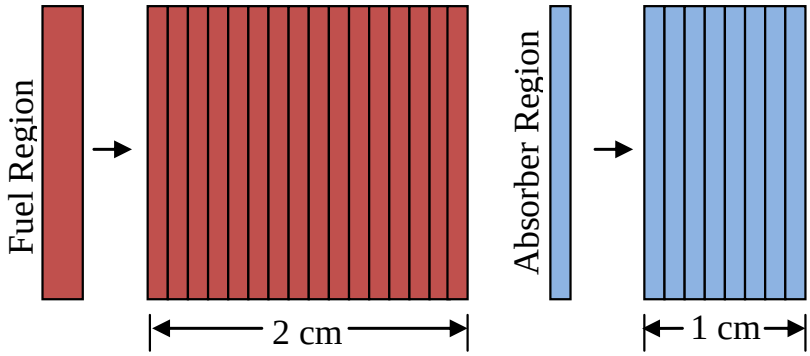

Figure 4: Problem 3: Regions

converging value of the cell-average Eddington factor are calculated and displayed for various choices of the number of Monte Carlo generations per QD solve (1, 5, 10, 25, 50, and 100). Figures 5, 6, 9 and 10 show that the statistical variation of the fission source calculated by the hybrid method decreases with the number of histories per generation and with the number of generations. This is a direct consequence of the reduced statistical variation in the Eddington Factors as the number of histories is increased. [See Figures 7 and 11.] This increase in histories can be obtained by increasing either the histories per generation or the number of generations averaged per QD solve - both lead to more accurate Eddington Factors and better overall results from the hybrid method.

The k-eigenvalue converged very quickly for Problem 1. Figures 8 and 12 show the statistical variation in the multiplication factor with the number of histories per Monte Carlo solve. Table 3 is a summary of the k-eigenvalues for the various simulations of Problem 1. The S_N solution for this problem using the S_{64} Gauss-Legendre angular quadrature and the simple corner balance spatial discretization on the same spatial mesh yields a k-eigenvalue of 0.99960, which is the same as all k-eigenvalues obtained from the hybrid method. The k-eigenvalue obtained from averaging the last 2000 generations of 2500 generations for analog MC using

5,000,000 histories per generation was 0.999576± 0.000438. In this test problem, the hybrid method was much more rapidly convergent than standard Monte Carlo. The computational power to run the analog MC problem was much greater than the hybrid runs and the result was a less precise and less accurate calculation of the k-eigenvalue. In additional analysis, it would be of value to make use of a computational timer to determine to greater accuracy the computational time difference between the two methods. In general an entire QD solve was as fast or faster than one MC generation. As a comparison, we look at the case using 1MC per QD solve, Table 3. Multiplying the number of MC solves by the number of histories per solve (25 x 50,000 = 1.25 x 10^6) and comparing with analog Monte Carlo (2500 x 5,000,000 = 1.25 x 10^{10}), we find that even the case using 1 MC generation per QD solve and 50,000 histories per generation, which according to the above approximation equaled approximately 2 x 10^{-4} the computational power, yielded a more accurate k-eigenvalue than analog MC with 2500 generations and 5,000,000 histories per generation.

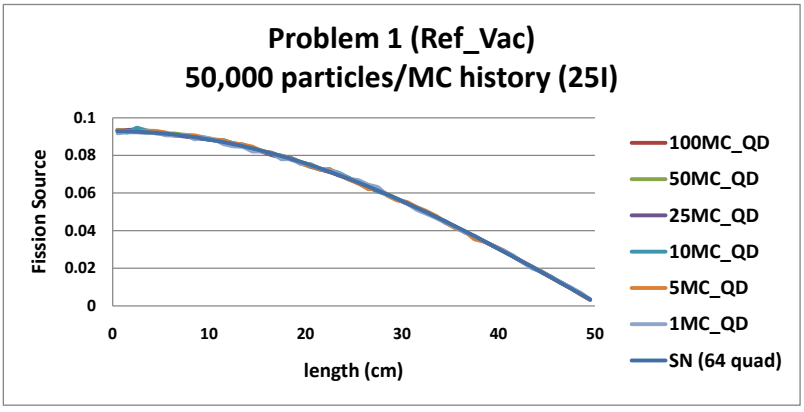

Figure 5: Problem 1: Fission source distribution with 50,000 particles per generation.

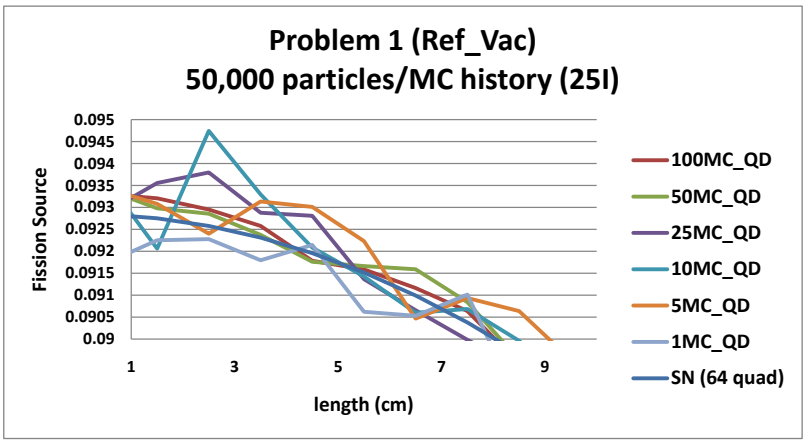

Figure 6: Problem 1: Fission source distribution with 50,000 particles per generation on the left edge of the slab.

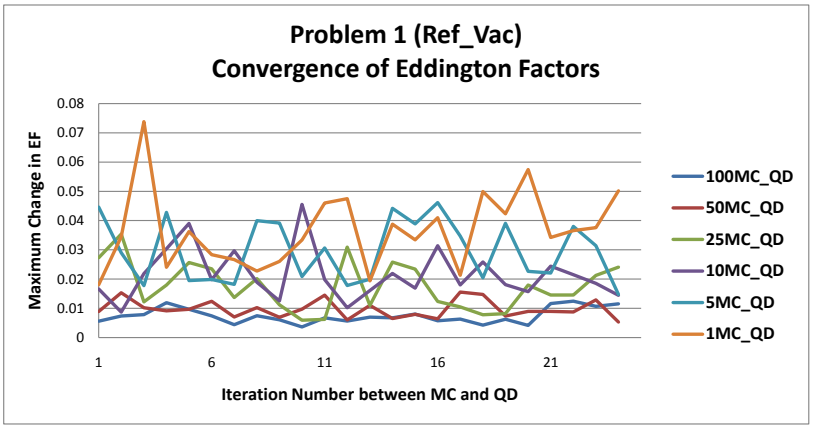

Figure 7: Problem 1: Convergence of Eddington factors with 50,000 particles per generation.

3.2.2 Test Problem #2

The results from Problem 2, with reflecting boundary on the left and a vacuum boundary on the right are shown in the figures below. We have performed calculations of this problem with 1600, 16000, 160000, and 1600000 particles per generation, and various choices for the number of Monte Carlo generations per QD solve.

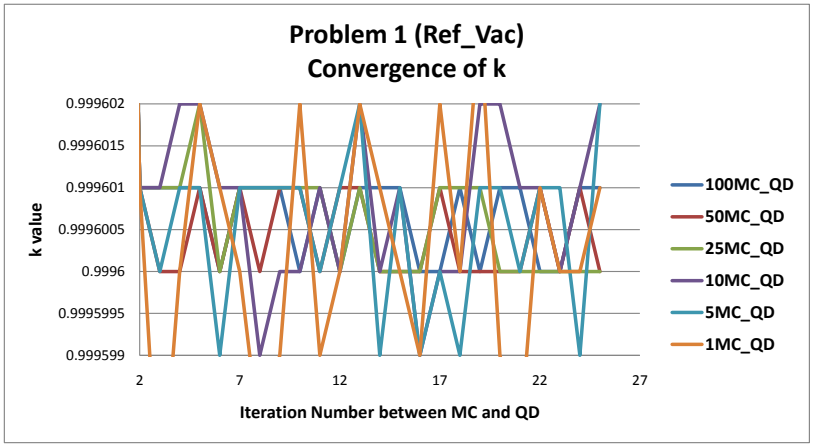

Figure 8: Problem 1: Convergence of the k-eigenvalue with 50,000 particles per generation.

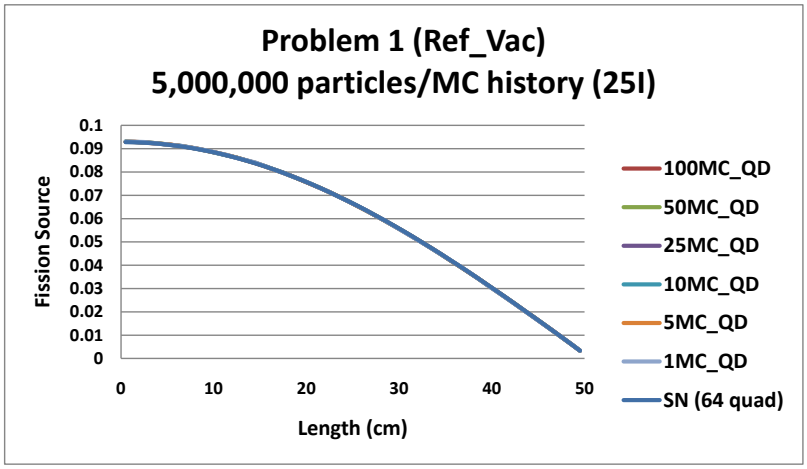

Figure 9: Problem 1: Fission source distribution with 5,000,000 particles per generation.

Figure 13 shows the fission source distribution for Problem 2 using 1600 particles per generation after a total of 25 QD solves. A closer view of the left edge of the slab is shown in Figure 14.

Increasing the number of particles per generation by two orders of magnitude further increases the accuracy of the fission source distribution, as shown in Figures 15 and 16 respectively.

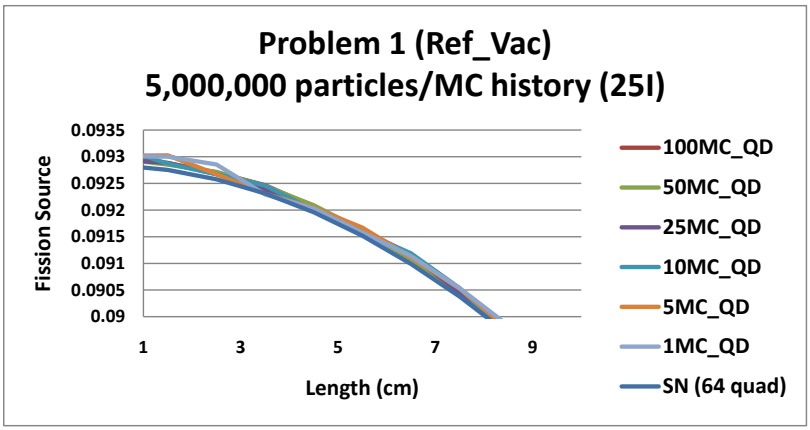

Figure 10: Problem 1: Fission source distribution with 5,000,000 particles per generation on the left edge of the slab.

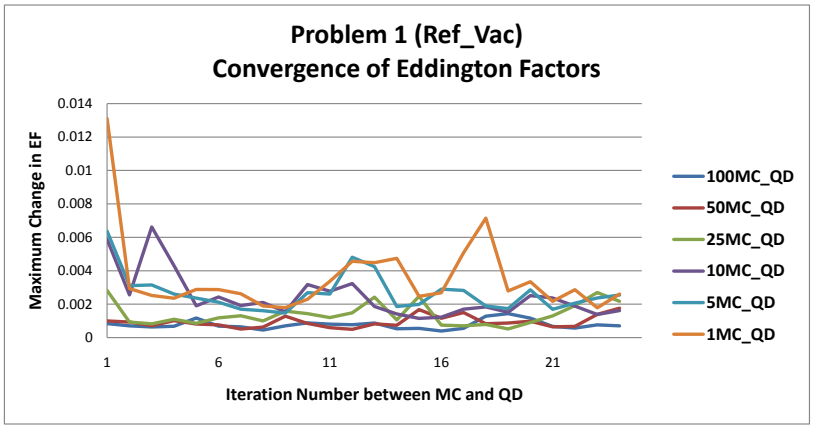

Figure 11: Problem 1: Convergence of Eddington factors with 5,000,000 particles per generation.

Figures 17 and 18 show the convergence of the slowest converging Eddington factor for Problem 2 with 1600 and 1600000 particles per generation and 1, 5, 20, 25, 50, and 100 averaged MC solves per QD solve. The Eddington factors for Problem 2 converge within a couple iterations. The fluctuations seen in the figures is a result of the statistical error in the MC calculation of the Eddington factors.

The multiplication factor was also found to converge quickly for Problem 2, as shown in Figures 19 and 20. The best estimate of the k-eigenvalue was found by

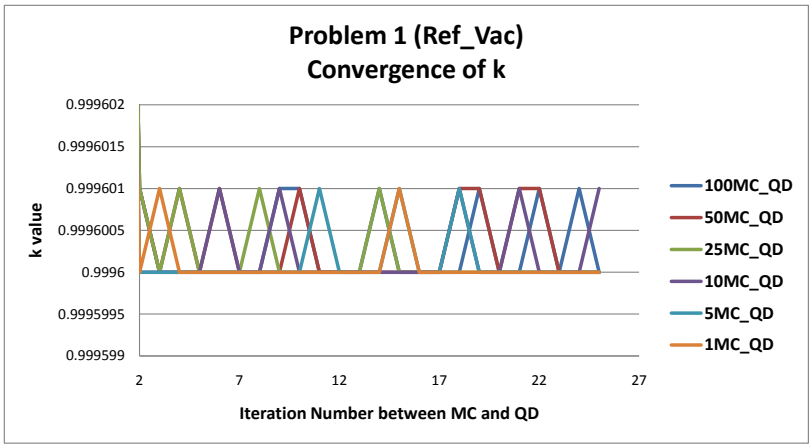

Figure 12: Problem 1: Convergence of the k-eigenvalue with 5,000,000 particles per generation.

Pr. 1	**50,000**	**500,000**	**5,000,000**
1	0.999600±1e-6	0.999600±5e-7	0.999600±3e-7
5	0.999601±9e-7	0.999600±5e-7	0.999600±3e-7
10	0.999601±9e-7	0.999600±5e-7	0.999600±4e-7
25	0.999601±6e-7	0.999601±5e-7	0.999600±4e-7
50	0.999600±5e-7	0.999600±5e-7	0.999600±5e-7
100	0.999601±5e-7	0.999600±4e-7	0.999600±5e-7

Table 3: k-eigenvalue (Problem 1); particles per generation vs. number of MC runs averaged per QD solve. Each k-eigenvalue is an average of the eigenvalues from 25 QD iterations.

averaging the results from each QD solve as shown in Table 4. The simple corner balance result, with S_{64} Gauss-Legendre quadrature, is 0.53217. The analog MC k-eigenvalue obtained with 464000 particles per generation and averaging the last 2000 of 2500 generations was 0.532209 ±0.000728. Both the S_N and analog MC eigenvalue fall within one standard deviation of all the k-eigenvalues listed in Table 4. This shows that the hybrid method performs well for calculating the k-eigenvalue of Problem 2 with a reflecting boundary on the left hand side and vacuum on the right.

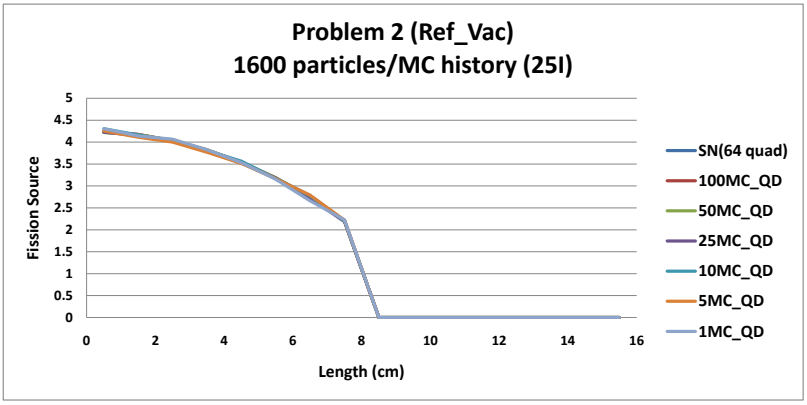

Figure 13: Problem 2: Fission source distribution after 25 QD iterations with 1600 particles per generation.

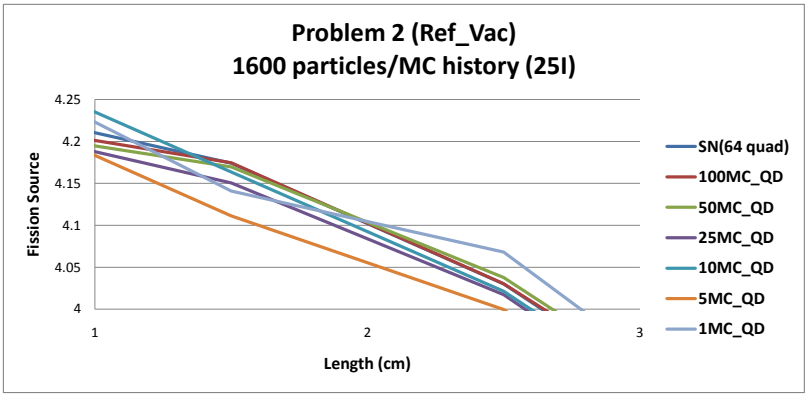

Figure 14: Problem 2: Fission source distribution on the left edge of the slab after 25 QD iterations with 1600 particles per generation.

3.2.3 Test Problem #2b

Problem 2b has the same material compositions as Problem 2, but with a vacuum boundary on the left and a reflecting boundary on the right. Figures 21 and 22 show the fission source distribution with 160,000 histories per MC generation and 1, 5, 10, 25, 50, and 100 MC generations per QD solve. As can be seen in the figures, the fission source distribution agrees well with that obtained from the simple corner balance method using the S_{64} Gauss-Legendre quadrature set. In addition the most widely varying Eddington factor and the k-eigenvalue converge

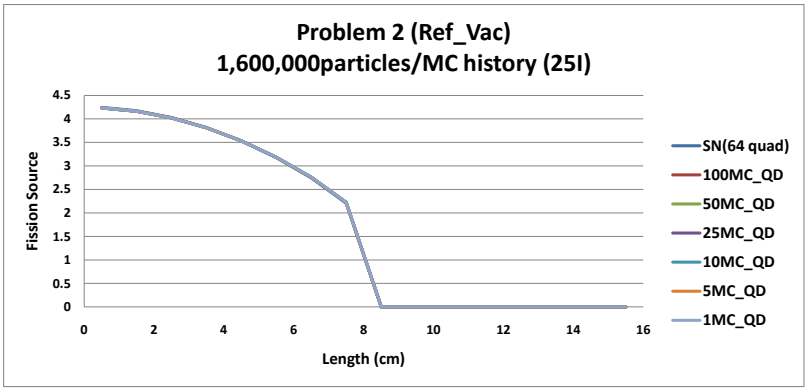

Figure 15: Problem 2: Fission source distribution with 1,600,000 particles per generation

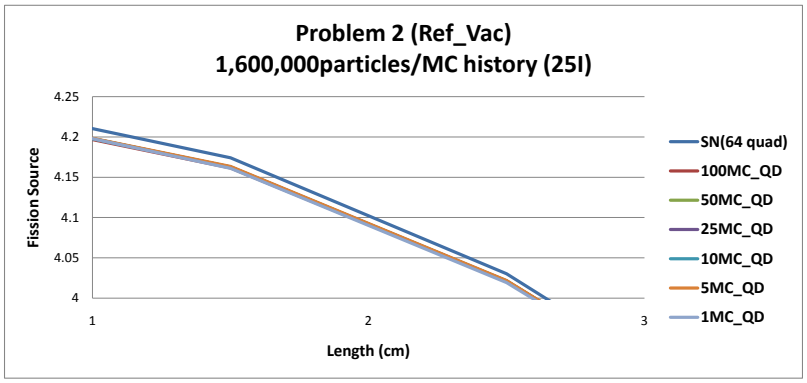

Figure 16: Problem 2: Fission source distribution on the left edge of the slab after 25 QD iterations with 1,600,000 particles per generation.

within the first couple iterations as shown in Figures 23 and 24.

The k-eigenvalue obtained from analog Monte Carlo with 160,000 histories per generation and a total of 10,000 generations was 0.342541±0.000824. This k-value is the average of the last 9500 generations; the first 500 were skipped. The multiplication factors obtained from the simple corner balance method with S_{64} and S_{128} angular quadratures were 0.34247 and 0.34251 respectively. Considering the error bars on the analog MC eigenvalue, it compares very well with the values obtained from the S_N method. Table 5 contains the eigenvalues from the hybrid method

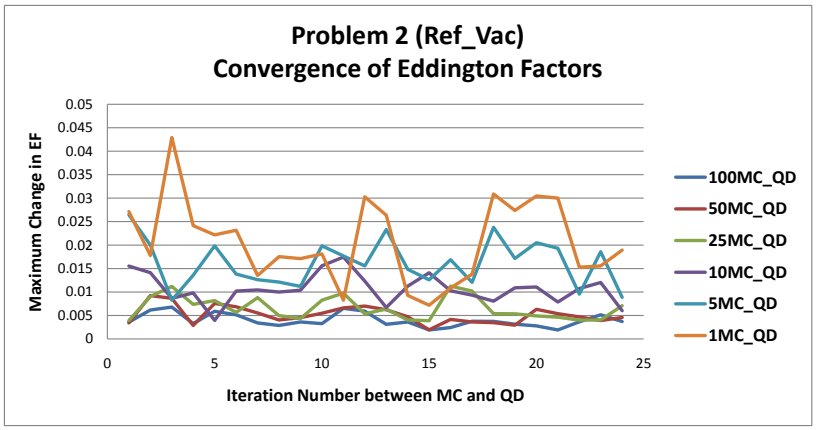

Figure 17: Problem 2: Convergence of the Eddington factor with 1600 particles per generation.

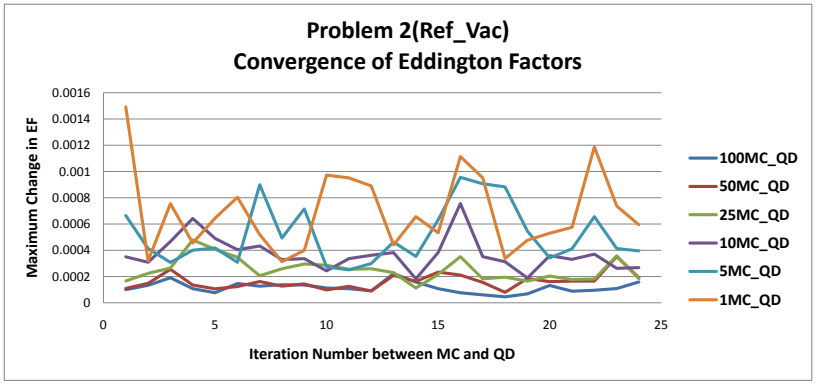

Figure 18: Problem 2: Convergence the of Eddington Factor with 1,600,000 particles per generation.

using 160,000 and 1,600,000 histories per MC generation and averaging 1, 5, 10, 25, 50, and 100 MC generations per QD generation after a total of 25 iterations. The MC/QD hybrid results differ in reactivity from the analog MC and SN methods by approximately \$0.90. It is possible that the strong gradient in the solution is not sufficiently resolved in the hybrid method calculation. We plan to increase the spatial resolution near the boundary to see if this effect is mitigated. As will be seen in the multigroup results, increasing the spatial resolution significantly increases the accuracy of many of the results.

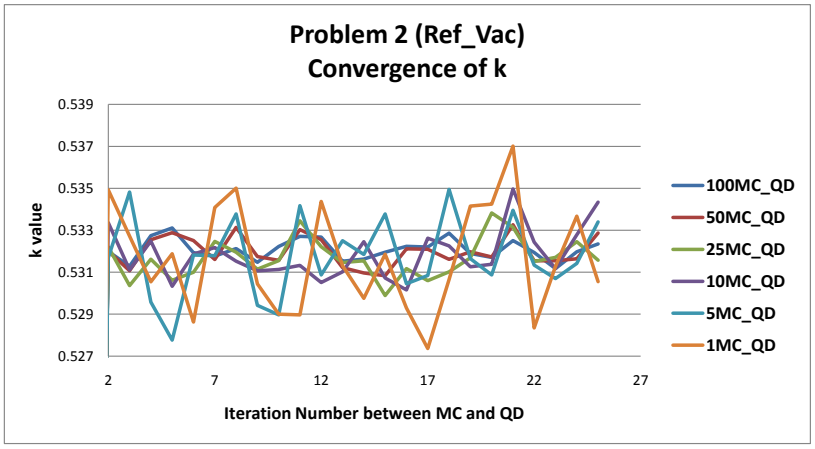

Figure 19: Problem 2: Convergence of the k-eigenvalue with 1600 particles per generation.

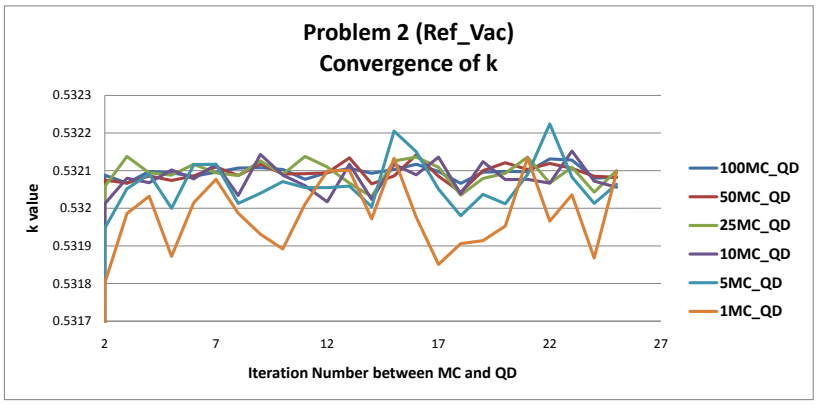

Figure 20: Problem 2: Convergence of the k-eigenvalue with 1,600,000 particles per generation.

3.2.4 Test Problem #3

Problem 3 is a difficult problem for standard analog Monte Carlo because of its high dominance ratio of approximately 0.996 [Urb. 1995]. We solve this problem with analog Monte Carlo with an initial fission source distribution that is twice as large in the right half of the problem as it is in the left half. Figures 25 and 26 show that the fission source distribution is converging very slowly over 20000 analog Monte Carlo generations.

Pr. 2	1600	16,000	160,000	1,600,000
1	0.531670±0.002549	0.531785±0.000799	0.532014±0.000301	0.531984±0.000093
5	0.531765±0.001878	0.531909±0.000682	0.532145±0.000239	0.532064±0.000065
10	0.531853±0.001200	0.532008±0.000550	0.532127±0.000144	0.532081±0.000040
25	0.531674±0.000945	0.532034±0.000281	0.532121±0.000107	0.532095±0.000032
50	0.532002±0.000706	0.532055±0.000222	0.532100±0.000066	0.532094±0.000023
100	0.532083±0.000505	0.532035±0.000168	0.532107±0.000043	0.532096±0.000016

Table 4: k-eigenvalue (Problem 2); particles per generation vs. number of MC runs averaged per QD solve. Each k-eigenvalue is an average of the eigenvalues from 25 QD iterations.

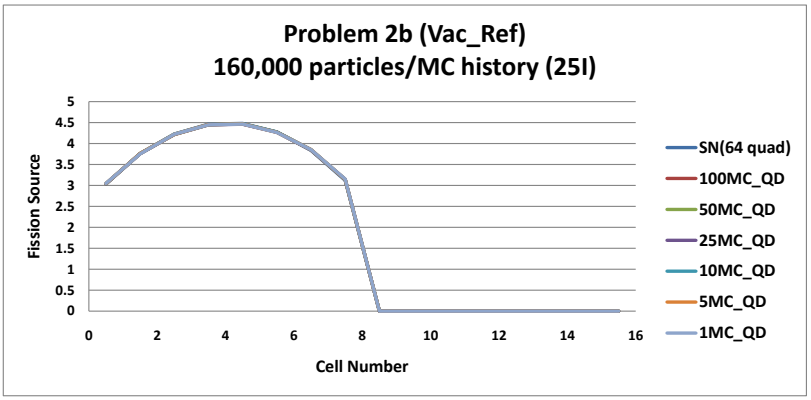

Figure 21: Problem 2b: Fission source distribution with160,000 particles per generation.

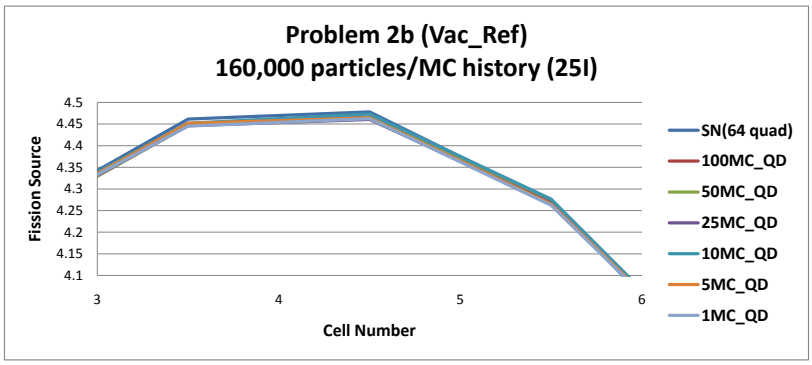

Figure 22: Problem 2b: Fission source distribution with 160,000 particles per generation on the left edge of the slab.

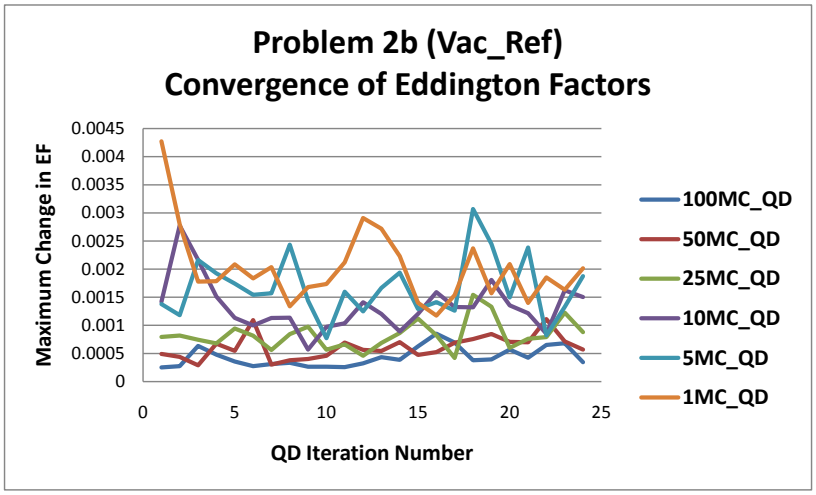

Figure 23: Problem 2b: Convergence of the k-eigenvalue with 160,000 particles per generation.

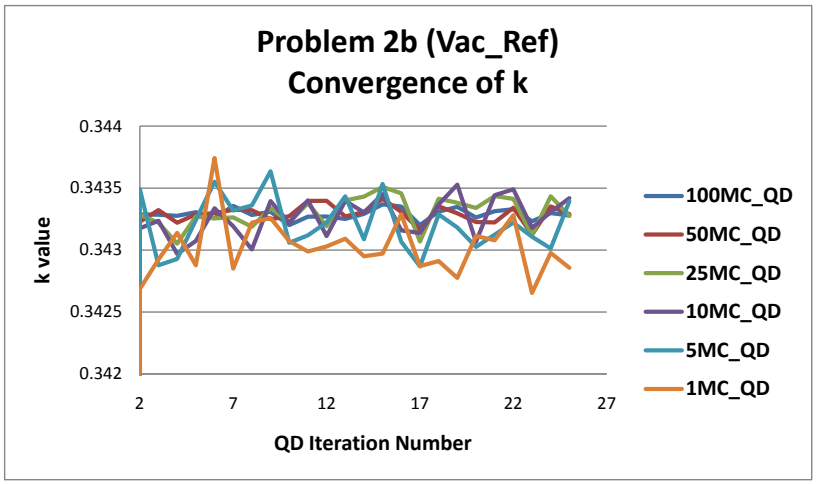

Figure 24: Problem 2b: Convergence of the k-eigenvalue with 160,000 particles per generation.

Figure 27 compares the fission source obtained from analog Monte Carlo and deterministic transport with S_{32}, S_{64}, and S_{128} angular quadratures. The MC fission source shown in Figure 27 was a result of 464000 histories per generation and a total of 20000 generations. The difference between the MC and S_N solutions is most likely caused by the Monte Carlo fission source not being sufficiently converged.

Pr. 2b	160,000	1,600,000
1	0.343026±0.000231	N/A
5	0.343215±0.000216	N/A
10	0.343265±0.000160	N/A
25	0.343307±0.000125	N/A
50	0.343291±0.000071	N/A
100	0.343289±0.000044	0.343293±0.000015

Table 5: k-eigenvalue (Problem 2b); particles per generation vs. number of MC runs averaged per QD solve. Each k-eigenvalue is an average of the eigenvalues from 25 QD iterations.

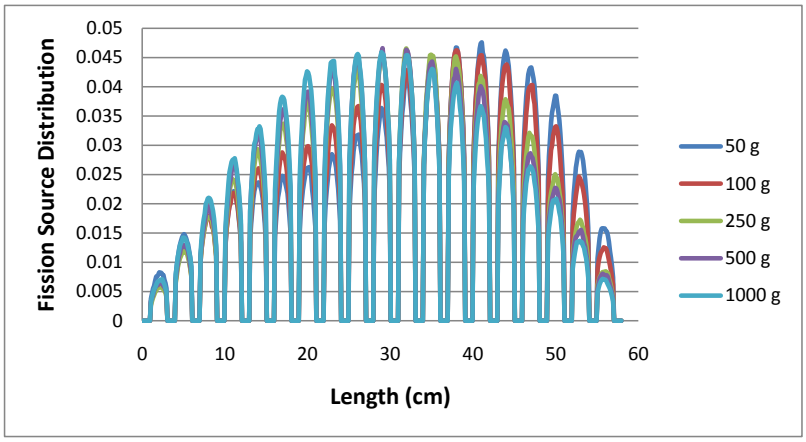

Figure 25: Problem 3: Convergence of the fission source with 50-1000 analog MC generations.

Figures 28, through 33 show the fission source distributions for Problem 3 with 1, 5, 10, 25, 50, and 100 MC generations per QD solve and 464,000 and 4,640,000 histories per MC generation. The largest cell-averaged difference between the S_N fission source distribution and fission source distribution obtained from the MC/QD hybrid method for 464,000 histories per MC generation is 15% for 1MC/QD iteration and 3.9% for 100MC/QD iteration. For MC/QD hybrid results using 4,640,000 histories per MC generation the largest difference is 3.5% for 1MC/QD and 1.8% for 100MC/QD. The hybrid method was employed with

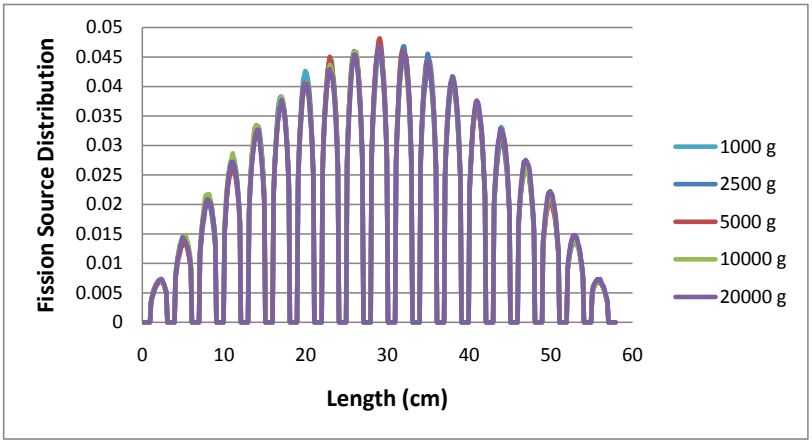

Figure 26: Problem 3: Convergence of the fission source with 1000-20000 analog MC generations.

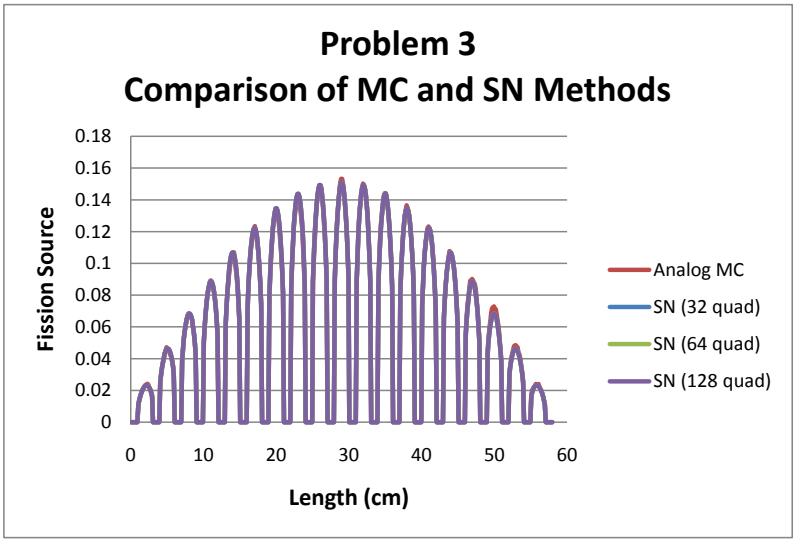

Figure 27: Problem 3: Comparison of the fission source distributions from S_N and analog Monte Carlo.

the initial fission source distribution skewed to the right as discussed above.

Figures 30 and 34 show the convergence of the most widely varying Eddington factor. The maximum change in the Eddington factors from iteration to iteration converges within the first couple iterations.

Similarly, Figures 31 and 35 show the convergence of the k-eigenvalue as a

function of the number of QD solves. The k-eigenvalue was also found to converge within the first few iterations. Table 6 shows the average k-eigenvalue for the problems shown in Figures 28 through 35. The k-eigenvalues obtained using the simple corner balance method with S_{32}, S_{64}, S_{128}, and S_{256} angular quadratures were 0.59908, 0.59918, 0.59920, and 0.59921 respectively. All these multiplication factors fall below those obtained from the hybrid method, though it does slightly increase with angular resolution. The analog Monte Carlo k-eigenvalue 464,000 histories per generation and a total of 20000 generations was 0.599214±0.000840. [The first 500 generations were skipped and the last 19500 generations were used in the eigenvalue averaging.] All the MC/QD runs fall within one standard deviation of the analog MC eigenvalue result.

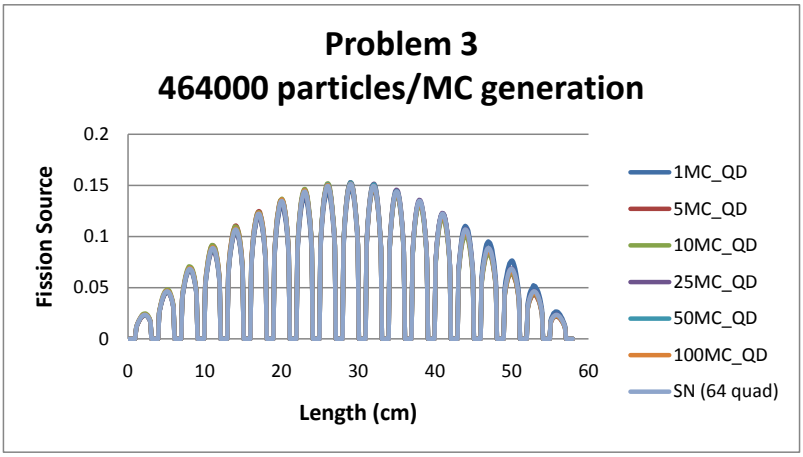

Figure 28: Problem 3: Fission source distribution with 464,000 histories per MC generation.

3.3 Multi-Group Results

Multi Group results will be shown for four different problems. Problem 4 is a homogeneous problem with two energy groups. This problem is composed of 16 cells, each 0.125 cm across. Table 7 contains the material properties for Problem

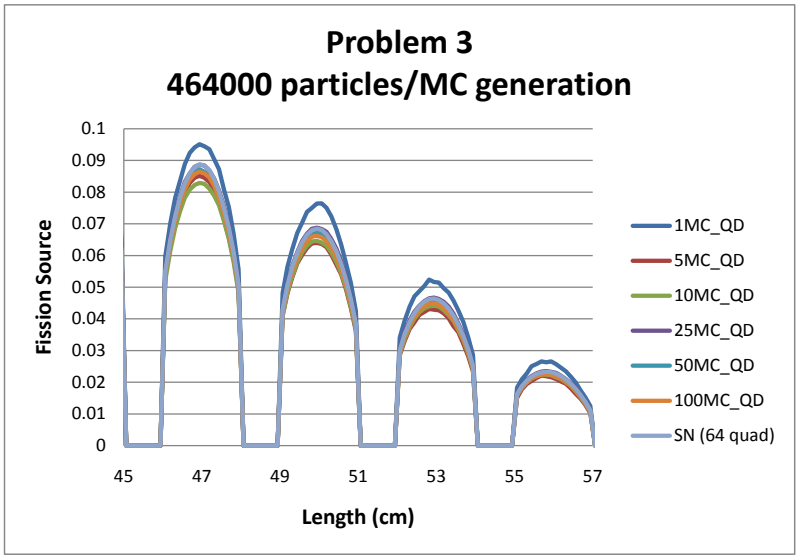

Figure 29: Problem 3: Fission source distribution on the right side of the slab with 464,000 histories per MC generation.

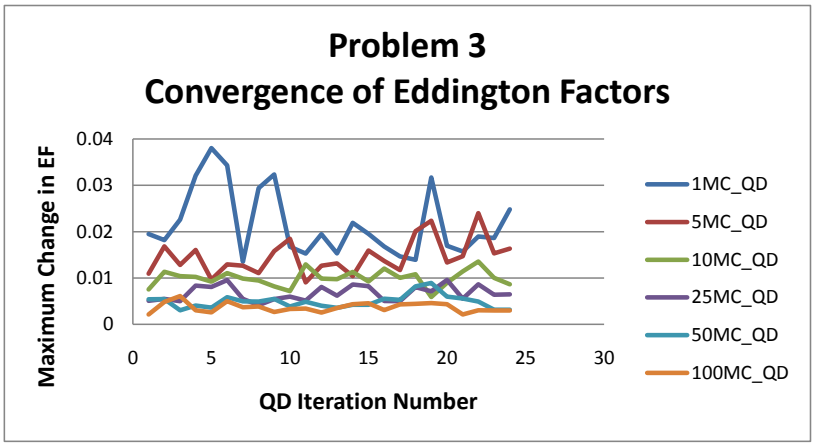

Figure 30: Problem 3: Convergence of the Eddington factors with 464,000 histories per MC generation.

4. We considered two variations of this problem: reflecting boundaries on both the left and right, and vacuum boundary on the left/reflecting boundary on the right. A pictorial representation of Problem 4 is shown below in Figure 36.

Problem 5 is a two region, two energy group problem comprised of 1.0 cm of fuel followed by 1.0 cm of absorber. The fuel and absorber regions are both broken

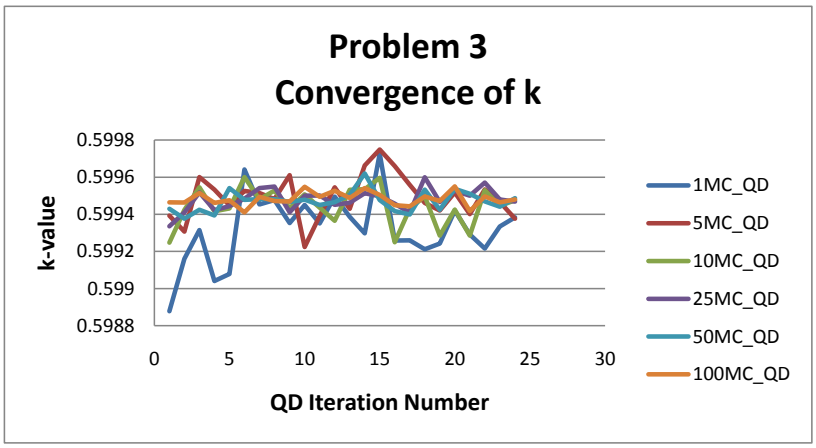

Figure 31: Problem 3: Convergence the of k-eigenvalue with 464,000 histories per MC generation.

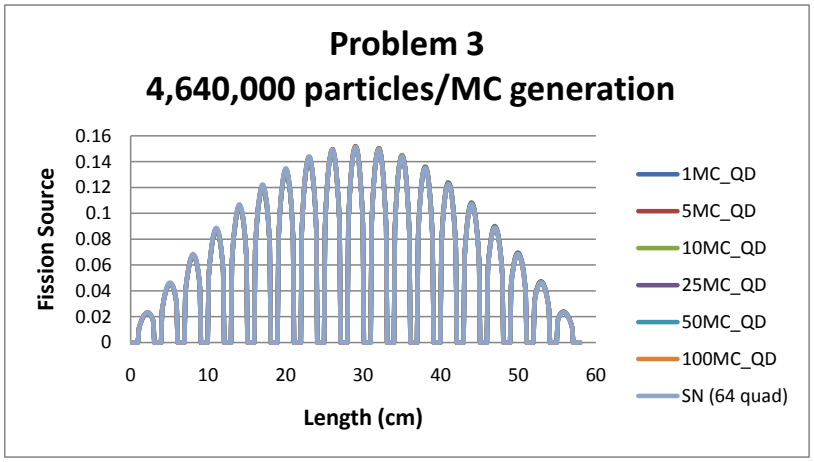

Figure 32: Problem 3: Fission source distribution with 4,640,000 histories per MC generation.

into 8 cells of length 0.125 cm. The material properties for both regions are shown in Table 8 Three variations of this problem are considered: reflecting boundaries on both the left and right, reflecting boundary on the left/vacuum boundary on the right, and vacuum boundary on the left/reflecting boundary on the right. A pictorial representation is shown in Figure 37.

Problem 6 is exactly the same as Problem 5 except each 0.125 cm cell is broken

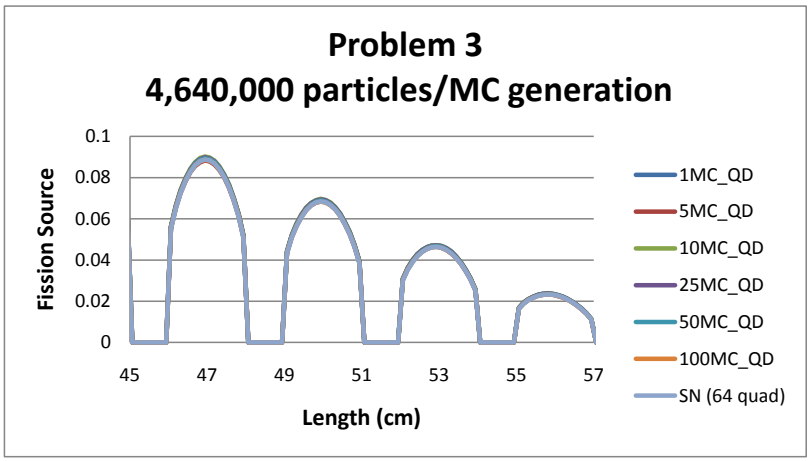

Figure 33: Problem 3: Fission source distribution on the right side of the slab with 4,640,000 histories per MC generation.

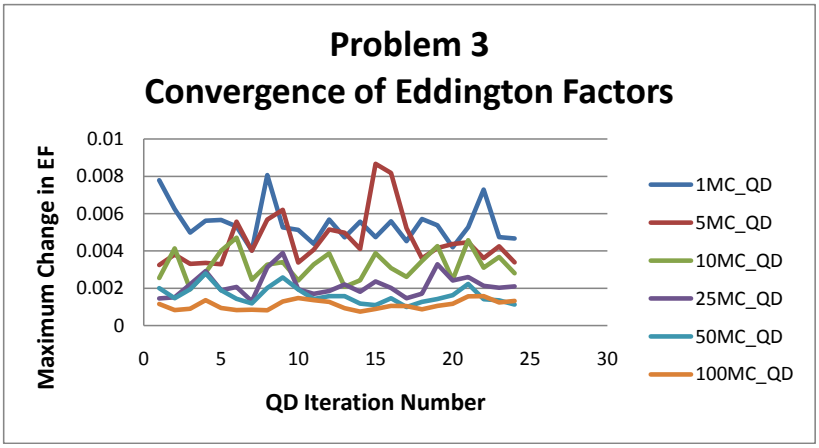

Figure 34: Problem 3: Convergence of the Eddington factors with 4,640,000 histories per MC generation.

into five 0.025 cm cells. All the same variations were considered as were considered in Problem 5.

Problem 7 is the same spatially as Problem 3. The cross-sections of fuel and moderator are the same as those of Problem 5. Both the left and right hand boundaries are vacuum. A pictorial representation of Problem 7 is shown in Figures 38 and 39.

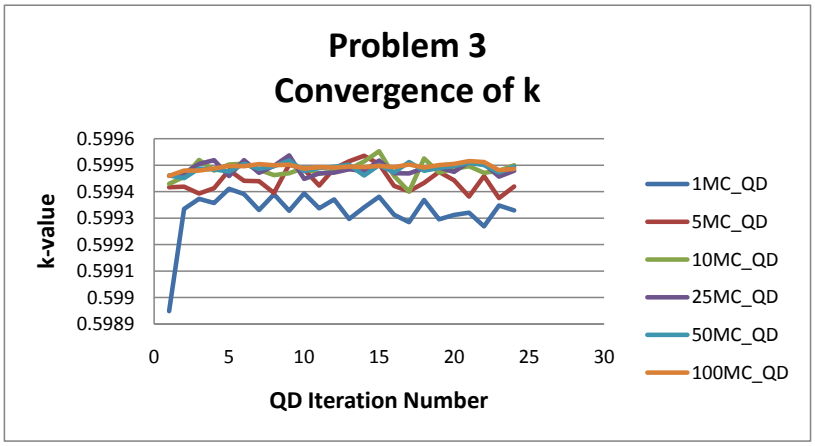

Figure 35: Problem 3: Convergence of the k-eigenvalue with 4,640,000 histories per MC generation.

Pr. 3	**464,000**	**4,640,000**
1	0.599322±0.000183	0.599326±0.000089
5	0.599492±0.000118	0.599444±0.000045
10	0.599446±0.000101	0.599483±0.000031
25	0.599480±0.000059	0.599486±0.000024
50	0.599471±0.000055	0.599488±0.000017
100	0.599483±0.000037	0.599494±0.000012

Table 6: k-eigenvalue (Problem 3); particles per generation vs. number of MC runs averaged per QD solve. Each k-eigenvalue is an average of the eigenvalues from 25 QD iterations.

Problem 8 is a two region problem with 4 energy groups. The problem is comprised of 1.0 cm of absorber, followed by 1.0 cm of fuel. Both the absorber and the fuel regions are divided into 8 equal cells, each 0.125 cm across. The cross sections for the fuel (region 1) and absorber (region 2) are shown in Table 9. Two different sets of boundary conditions were analyzed for this problem: both boundaries reflecting, and right hand boundary condition vacuum/left boundary condition reflecting. Figure 40 is a pictorial representation of Problem 8.

Problem 9 is the same as Problem 8, except that each 0.125 cm cell is broken

Region	Σ_{t1}	$\Sigma_{s1\rightarrow1}$	$\Sigma_{s1\rightarrow2}$	$\nu\Sigma_f1$
1	1.5	0.5	0.8	0.0
	Σ_{t2}	$\Sigma_{s2\rightarrow1}$	$\Sigma_{s2\rightarrow2}$	$\nu\Sigma_f2$
	1.5	0.0	0.3	0.8

Table 7: Material Properties (Problem 4)

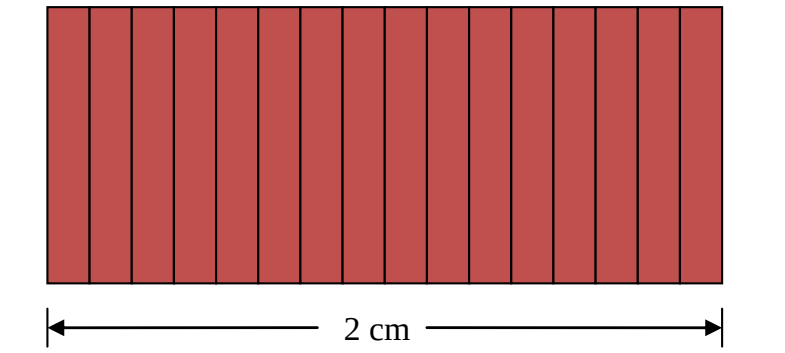

Figure 36: Problem 4

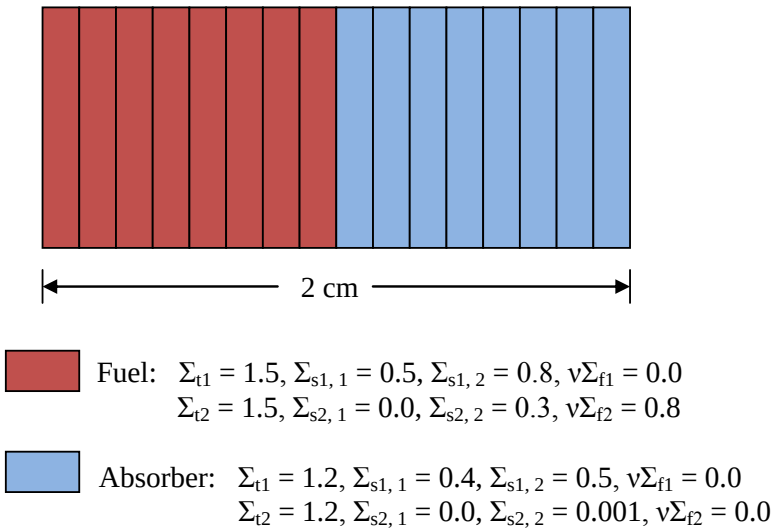

Figure 37: Problem 5

Region	**1**	**2**
Σ_{t1}	1.5	1.2
$\Sigma_{s1\rightarrow 1}$	0.5	0.4
$\Sigma_{s1\rightarrow 2}$	0.8	0.5
$\nu\Sigma_{f1}$	0.0	0.0
Σ_{t2}	1.5	1.2
$\Sigma_{s2\rightarrow 1}$	0.0	0.0
$\Sigma_{s2\rightarrow 2}$	0.3	0.001
$\nu\Sigma_{f2}$	0.8	0.0

Table 8: Material Properties (Problem 5)

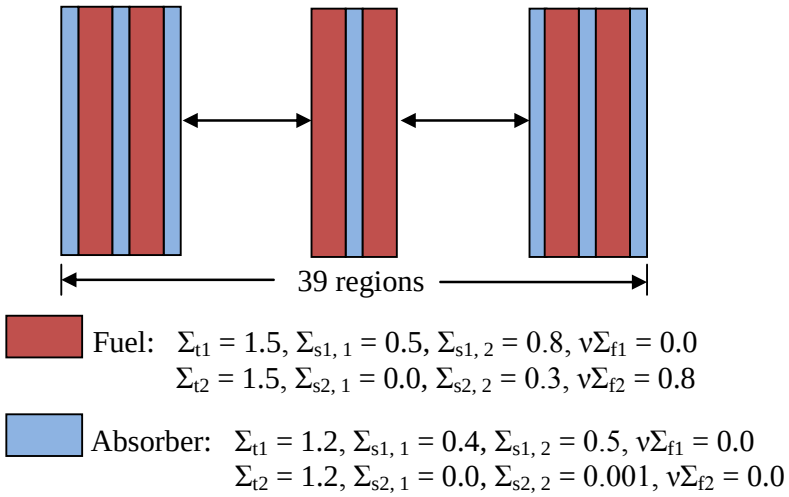

Figure 38: Problem 7

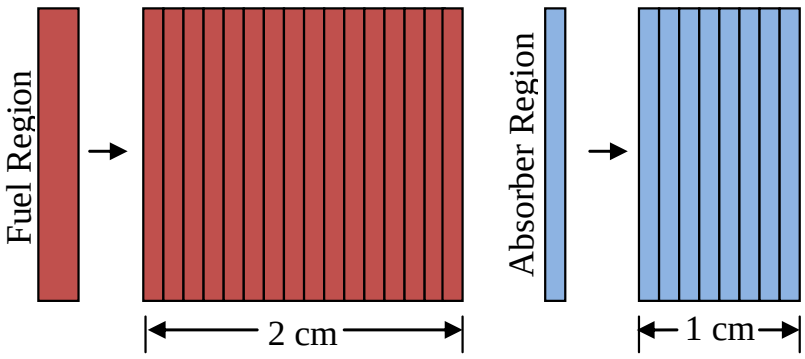

Figure 39: Problem 7: Regions

Region	1	2	Region	1	2
Σ_{t1}	1.5	1.2	Σ_{t3}	1.5	1.2
$\Sigma_{s1\rightarrow1}$	0.1	0.1	$\Sigma_{s3\rightarrow1}$	0.0	0.0
$\Sigma_{s1\rightarrow2}$	0.5	0.5	$\Sigma_{s3\rightarrow2}$	0.0	0.0
$\Sigma_{s1\rightarrow3}$	0.2	0.2	$\Sigma_{s3\rightarrow3}$	0.5	0.05
$\Sigma_{s1\rightarrow4}$	0.2	0.2	$\Sigma_{s3\rightarrow4}$	0.5	0.15
$\nu\Sigma_{f1}$	0.0	0.0	$\nu\Sigma_{f3}$	0.0	0.0
Σ_{t2}	1.5	1.2	Σ_{t4}	1.5	1.2
$\Sigma_{s2\rightarrow1}$	0.0	0.0	$\Sigma_{s4\rightarrow1}$	0.0	0.0
$\Sigma_{s2\rightarrow2}$	0.1	0.1	$\Sigma_{s4\rightarrow2}$	0.0	0.0
$\Sigma_{s2\rightarrow3}$	0.6	0.6	$\Sigma_{s4\rightarrow3}$	0.0	0.0
$\Sigma_{s2\rightarrow4}$	0.4	0.2	$\Sigma_{s4\rightarrow4}$	0.5	0.001
$\nu\Sigma_{f2}$	0.0	0.0	$\nu\Sigma_{f4}$	0.8	0.0

Table 9: Material Properties (Problem 8)

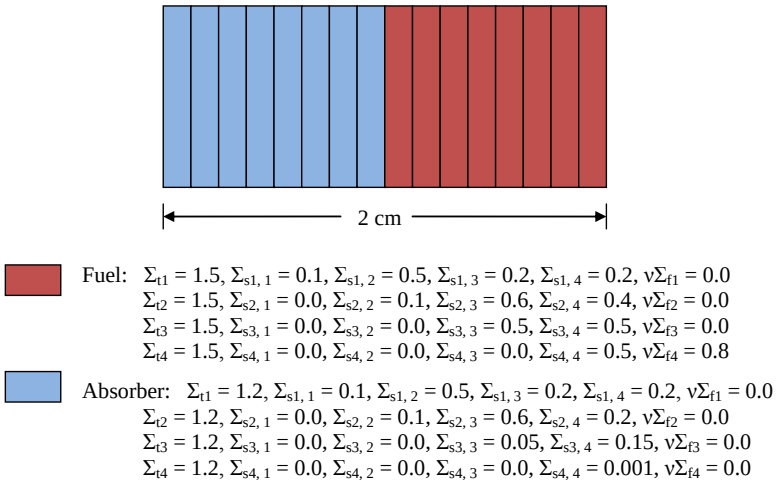

Figure 40: Problem 8

into 5 cells of 0.025 cm in width.

3.3.1 Test Problem #4a

Problem 4a (Problem 4 with both boundaries reflecting) was solved using 320,000 histories per MC generation. The fission source distribution and slowest converging value of the cell-averaged Eddington factor are calculated and displayed in Figures

41 and 42 for various choices of the number of Monte Carlo generations per QD solve (1, 5, 10, and 25). The k-eigenvalue converged exactly to 0.533333 in the first iteration for all simulations.

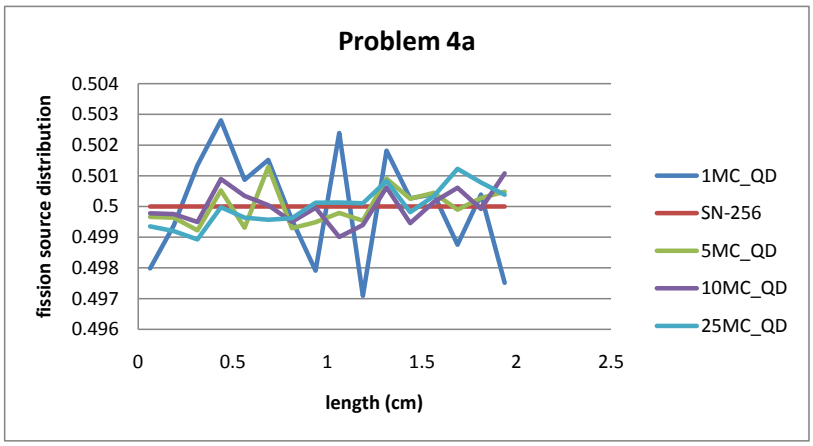

Figure 41: Problem 4a: Fission source distribution with 320,000 particles per generation

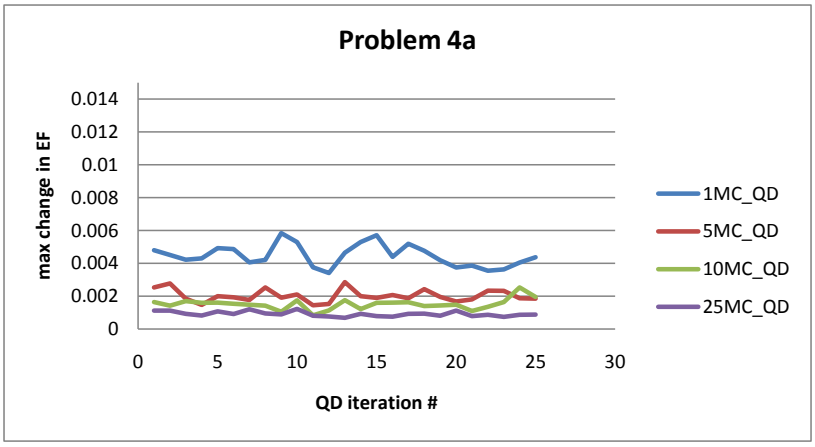

Figure 42: Problem 4a: Convergence of Eddington factors with 320,000 particles per generation.

3.3.2 Test Problem #4b

Problem 4b (Problem 4 with left boundary vacuum/right boundary reflecting) was solved using 320,000 histories per MC generation. The fission source, multiplication

factor, and slowest converging value of the EF are shown in Figures 43 through 46.

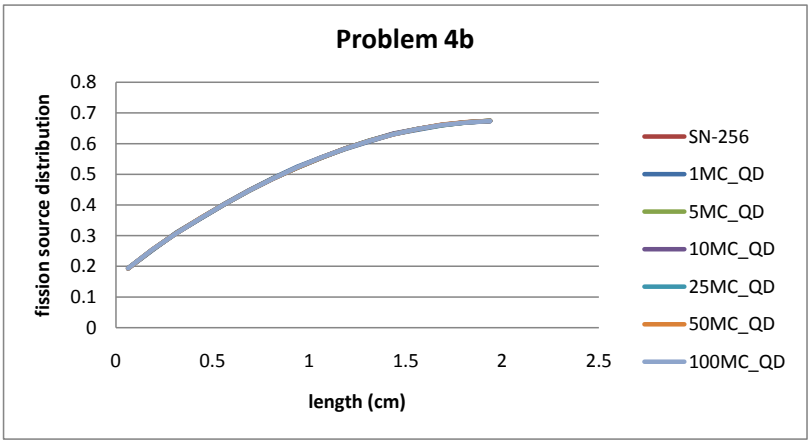

Figure 43: Problem 4b: Fission distribution with 320,000 histories per MC generation.

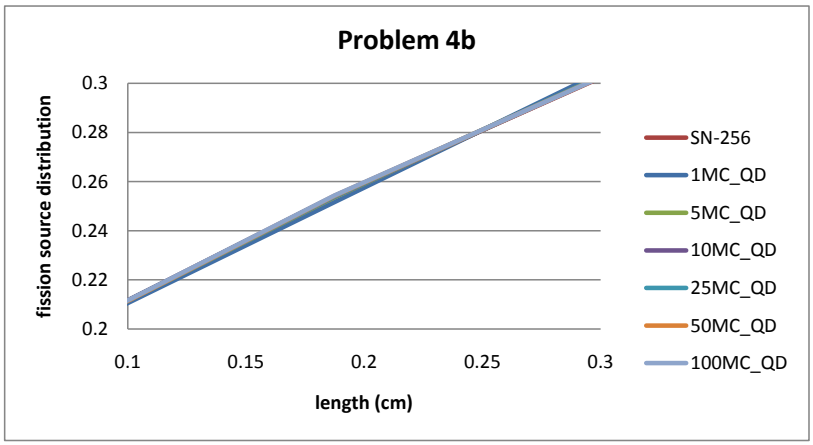

Figure 44: Problem 4b: Fission distribution with 320,000 histories per MC generation at left edge.

Table 10 shows the average of the eigenvalue from 25 QD iterations. The S_{256} Gauss-Legendre angular quadrature and the simple corner balance spatial discretization on the same spatial mesh yields a k-eigenvalue of 0.45713. As can be seen in Table 10 the MC/QD hybrid method predicted the k-eigenvalue accurately

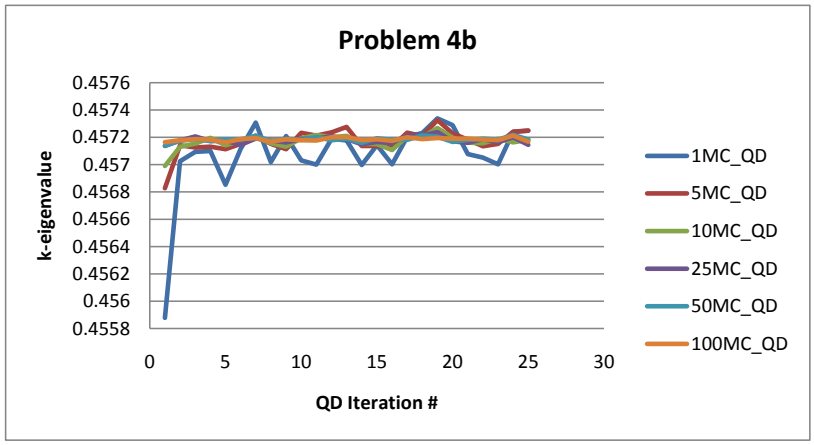

Figure 45: Problem 4b: Convergence of k-eigenvalue with 320,000 histories per MC generation.

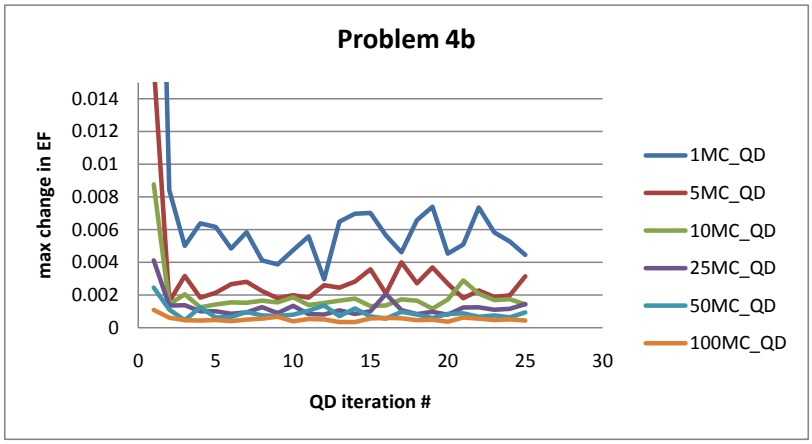

Figure 46: Problem 4b: Convergence of Eddington factors with 320,000 histories per MC generation.

to 4 significant figures, but was consistently high in the 5th significant figure. The reactivity difference predicted between the S_{256} method and the MC/QD method was approximately \$0.03. This difference is mostly likely a result of an unresolved spatial discretization. The Gauss-Legendre angular quadrature method with simple corner balance spatial discretization is locally 3rd order, globally 2nd order accurate and the finite volume discretization of the QD low order equations is locally 2nd order, globally 1st order accurate. For this reason the MC/QD method has a

greater truncation error in the spacial discretization.

Pr. 4b	320,000
1	0.457073±0.000276
5	0.457171±0.000092
10	0.457169±0.000051
25	0.457179±0.000025
50	0.457185±0.000017
100	0.457185±0.000012

Table 10: k-eigenvalue (Problem 4b); particles per generation vs. number of MC runs averaged per QD solve. Each k-eigenvalue is an average of the eigenvalues from 25 QD iterations.

3.3.3 Test Problems #5a, 5b, and 5c

Problem 5a (Problem 5 with both boundaries reflecting), 5b (Problem 5 with left boundary reflecting/right boundary vacuum), and 5c (Problem 5 with left boundary vacuum/right boundary vacuum) were solved using 320,000 histories per MC generation. In each case the fission source distribution, multiplication factor, and slowest converging value of the cell-averaged Eddington factor are calculated and displayed in Figures 47 through 57 for various choices of the number of Monte Carlo generations per QD solve (1, 5, 10, 25, 50, and 100). The S_{256} Gauss-Legendre angular quadrature and the simple corner balance spatial discretization on the same spatial mesh yields 0.38139, 0.37159, and 0.24695 for Problems 5a, 5b, and 5c respectively. The MC/QD using 100 Monte Carlo generations per QD solve predicted the k-eigenvalue higher, Table 11, then the S_{256} Gauss-Legendre angular quadrature method with simple corner balance spatial discretization by 0.13%, 0.13%, and 0.43%, respectively and subsequently a reactivity difference of \$0.49, \$0.50, and \$2.53, respectively. Refining the mesh improved the accuracy of the MC/QD result as will be shown in Problem 6.

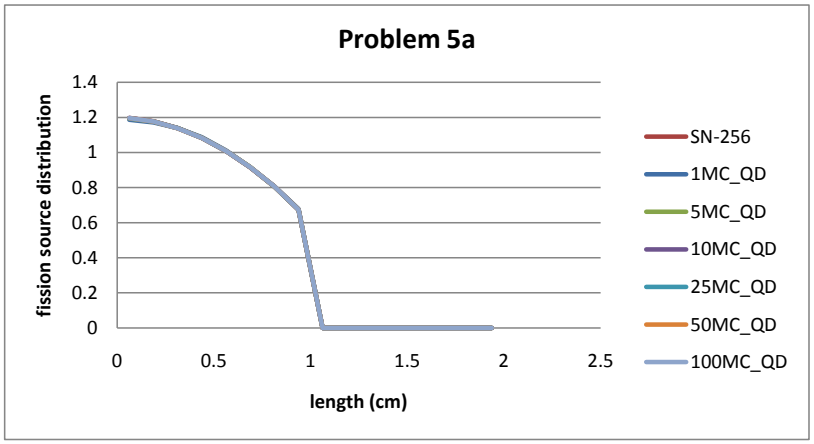

Figure 47: Problem 5a: Fission distribution with 320,000 histories per MC generation.

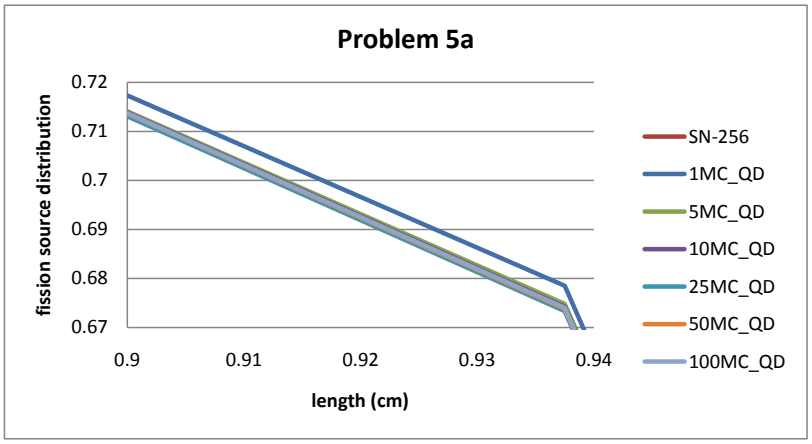

Figure 48: Problem 5a: Fission distribution with 320,000 histories per MC generation in the middle of the slab.

3.3.4 Test Problems #6a, 6b, and 6c

Problem 6a (Problem 6 with both boundaries reflecting), 6b (Problem 6 with left boundary reflecting/right boundary vacuum), and 6c (Problem 6 with left boundary vacuum/right boundary vacuum) were solved using 320,000 histories per MC generation. In each case the fission source distribution, multiplication factor, and slowest converging value of the cell-averaged Eddington factor were calculated for various choices of the number of Monte Carlo generations per QD solve (1, 5,

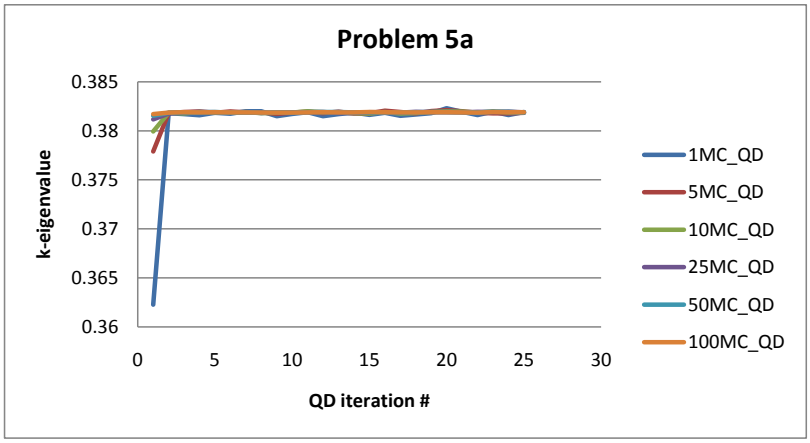

Figure 49: Problem 5a: Convergence of k-eigenvalue with 320,000 histories per MC generation.

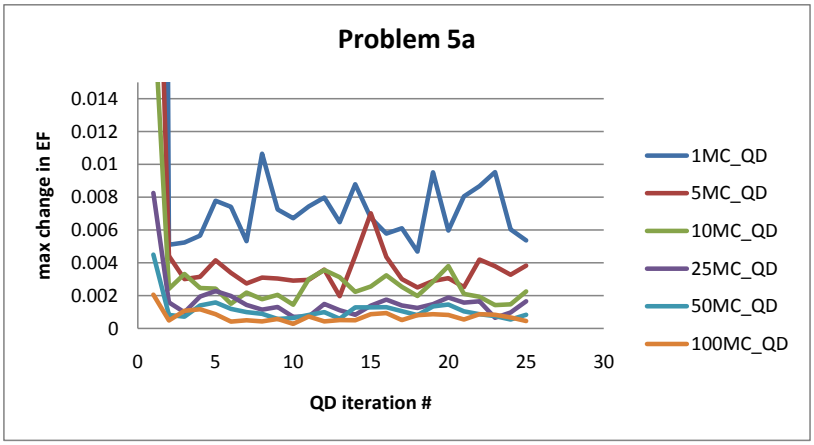

Figure 50: Problem 5a: Convergence of Eddington factors with 320,000 histories per MC generation.

10, 25, 50, and 100). Table 12 shows the k-eigenvalue obtained for each MC/QD run.

The S_{256} Gauss-Legendre angular quadrature and the simple corner balance spatial discretization on the same spatial mesh yields 0.38139, 0.37159, and 0.24695 for Problems 6a, 6b, and 6c respectively. The MC/QD using 100 Monte Carlo generations per QD solve predicted the k-eigenvalue higher then the S_{256} Gauss-Legendre angular quadrature method with simple corner balance spatial discretiza-

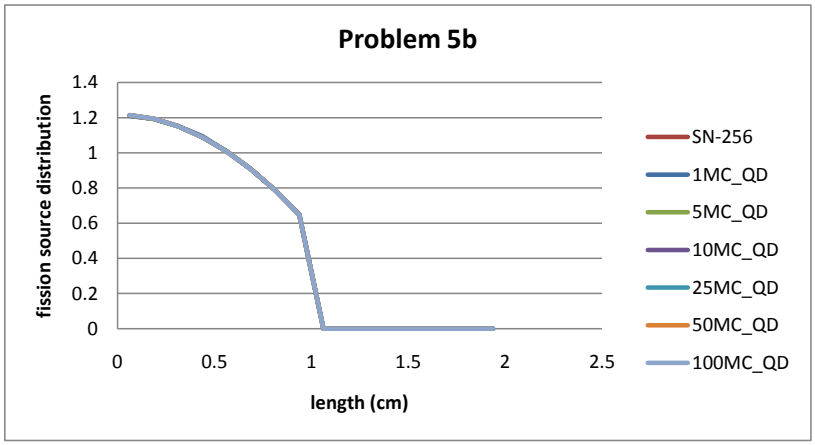

Figure 51: Problem 5b: Fission distribution with 320,000 histories per MC generation.

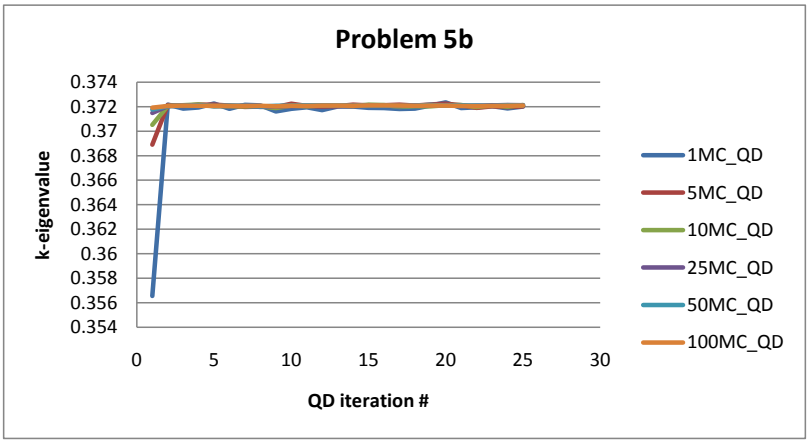

Figure 52: Problem 5b: Convergence of k-eigenvalue with 320,000 histories per MC generation.

tion, resulting in a reactivity difference of \$0.015, \$0.015, and \$0.10, respectively. As can be seen in comparison with Problem 5, Table 12, refining the mesh improved the accuracy of the MC/QD result significantly.

3.3.5 Test Problems #7

Problem 7 was solved using 4,640,000 histories per MC generation. In each case the fission source distribution, multiplication factor, and slowest converging value

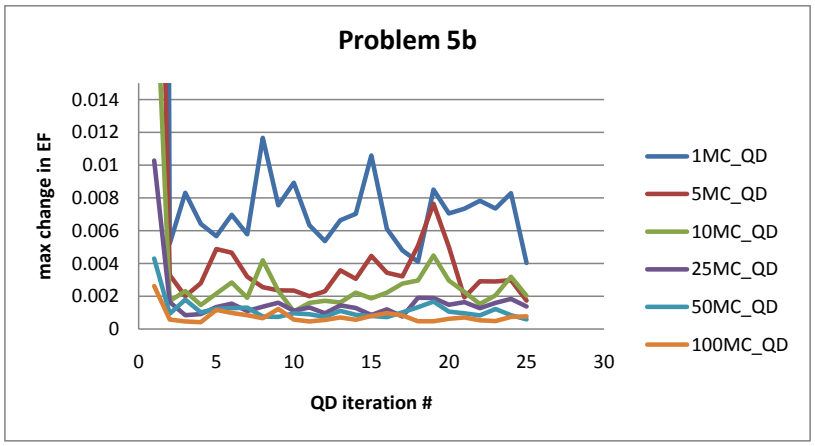

Figure 53: Problem 5b: Convergence of Eddington factors with 320,000 histories per MC generation.

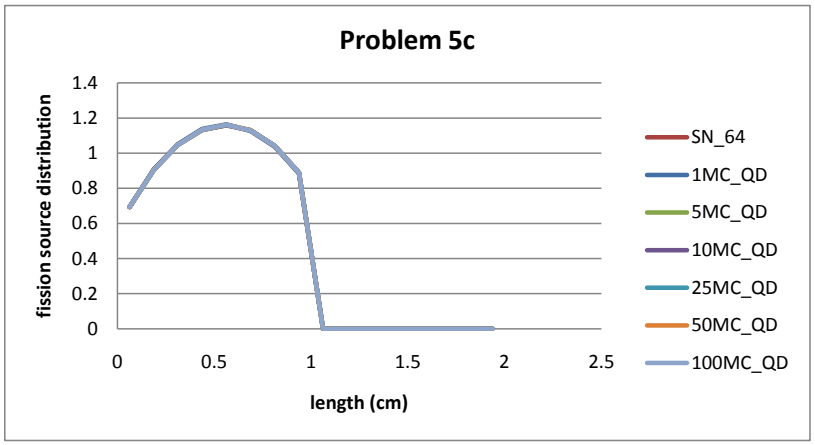

Figure 54: Problem 5c: Fission distribution with 320,000 histories per MC generation.

of the cell-averaged Eddington factor are calculated and displayed in Figures 58 through 64 for various choices of the number of Monte Carlo generations per QD solve (1, 5, 10, and 25). Table 13 shows the k-eigenvalues for each QD/MC run. S_{256} Gauss-Legendre angular quadrature method with simple corner balance spatial discretization gave a k-eigenvalue of 0.40648. The k-eigenvalue obtained for the QD/MC method using 25 MC generations per QD solve was 0.406899±1.35e-4. The reactivity difference between the QD/MC method using 25 MC generations

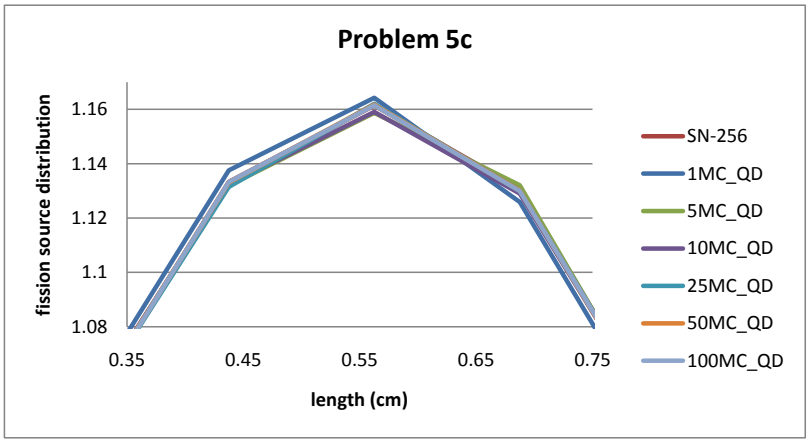

Figure 55: Problem 5c: Fission distribution with 320,000 histories per MC generation in the middle of the slab.

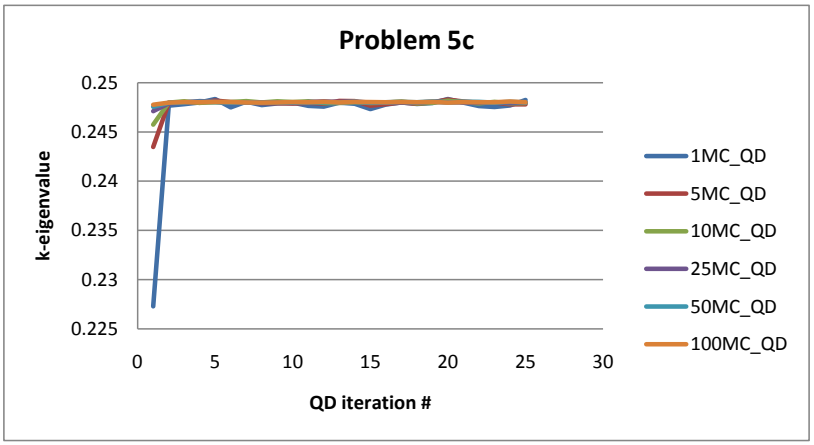

Figure 56: Problem 5c: Convergence of k-eigenvalue with 320,000 histories per MC generation.

per QD solve was \$0.37. Refining the mesh for the QD/MC method resulted in a more accurate k-eigenvalue as will be shown in Problem 7b.

3.3.6 Test Problems #7b

Problem 7 was solved using 4,640,000 histories per MC generation. In each case the fission source distribution, multiplication factor, and slowest converging value of the cell-averaged Eddington factor are calculated for various choices of the number

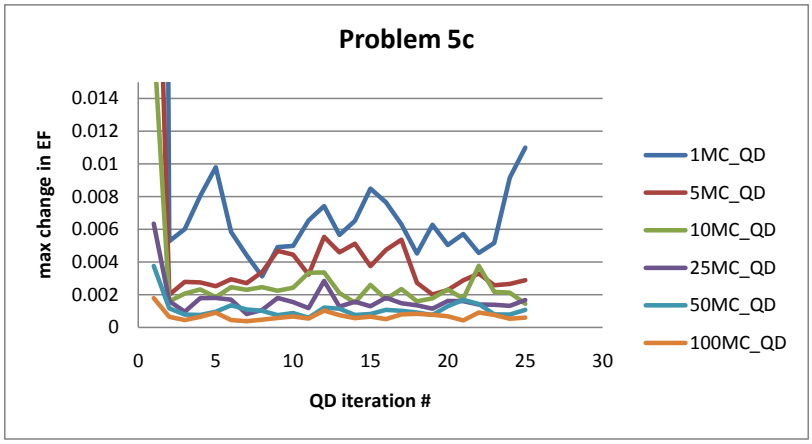

Figure 57: Problem 5c: Convergence of Eddington factors with 320,000 histories per MC generation.

Pr. 5	**5a**	**5b**	**5c**
1	0.380999±0.00391	0.371345±0.00309	0.247028±0.00412
5	0.381726±0.000803	0.371958±0.000643	0.247791±0.000908
10	0.381798±0.000392	0.372003±0.000315	0.247921±0.000459
25	0.381858±0.000151	0.372055±0.000125	0.247974±0.000186
50	0.381879±0.000075	0.372070±0.000070	0.248000±0.000099
100	0.381881±0.000040	0.372069±0.000036	0.248013±0.000060

Table 11: k-eigenvalue (Problem 5); Each MC run was done with 320,000 histories per generation and each k-eigenvalue is an average of the eigenvalues from 25 QD iterations.

of Monte Carlo generations per QD solve (1, 5, 10, and 25). Table 14 shows the k-eigenvalues for each QD/MC run. S_{256} Gauss-Legendre angular quadrature method with simple corner balance spatial discretization gave a k-eigenvalue of 0.40648. The k-eigenvalue obtained for the QD/MC method using 25 MC generations per QD solve was 0.406475±1.36e-4. The reactivity difference between the QD/MC method using 25 MC generations per QD solve was \$0.004. As can bee seen comparing Problem 7 with Problem 7b, refining the mesh for the QD/MC method resulted in a more accurate k-eigenvalue.

Pr. 6	6a	6b	6c
1	0.380631±0.00393	0.371002±0.00305	0.246145±0.00413
5	0.381250±0.000824	0.371482±0.000631	0.246836±0.000864
10	0.381338±0.000419	0.371551±0.000310	0.246908±0.000444
25	0.381383±0.000167	0.371588±0.000139	0.246964±0.000187
50	0.381399±0.000085	0.371598±0.000067	0.246977±0.000087
100	0.381405±0.000047	0.371604±0.000040	0.246992±0.000045

Table 12: k-eigenvalue (Problem 6); Each MC run was done with 320,000 histories per generation and each k-eigenvalue is an average of the eigenvalues from 25 QD iterations.

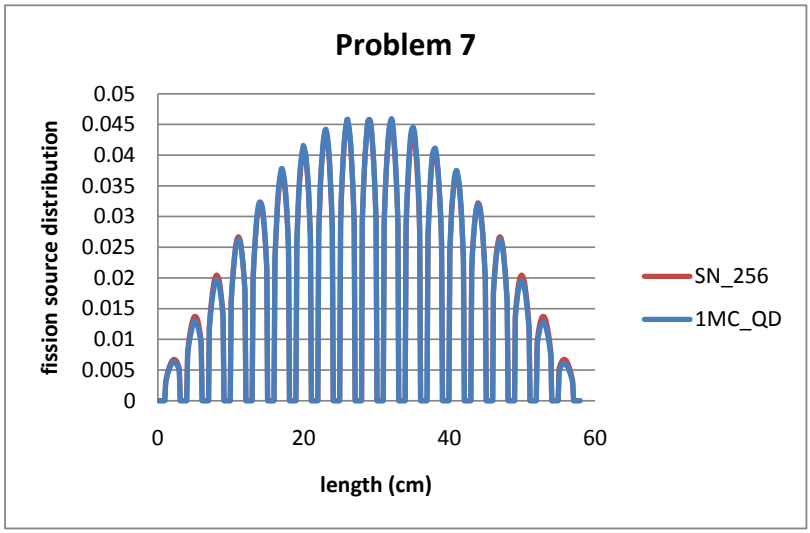

Figure 58: Problem 7: Fission distribution with 4,640,000 histories per MC generation and 1 MC generation/QD iteration.

3.3.7 Test Problems #8a and 8b

The results for Problem 8a (Problem 8 with both boundaries reflecting) and Problem 8b (Problem 8 with left boundary vacuum/right boundary reflecting) are shown in the figures below. We have performed calculations of this problem with 16000, 160000, and 1600000 histories per generation, and choices of 1, 5, 10, 25, 50, and 100 Monte Carlo generations per QD solve.

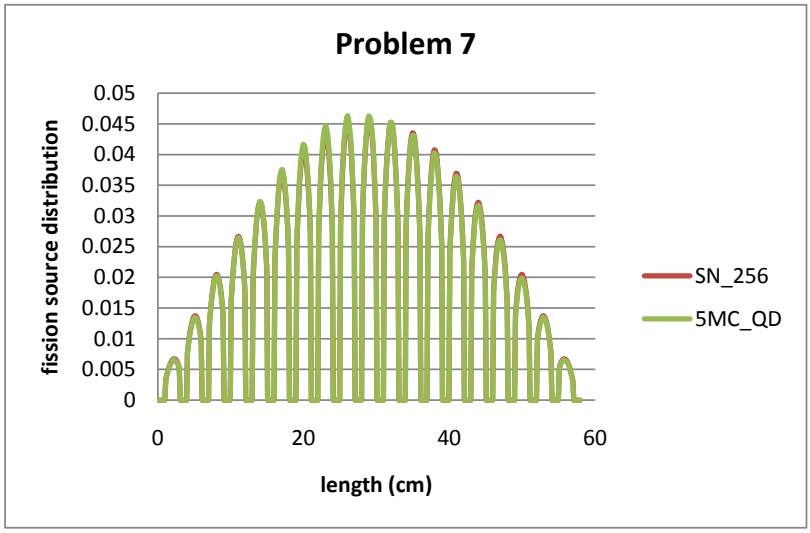

Figure 59: Problem 7: Fission distribution with 4,640,000 histories per MC generation and 5 MC generation/QD iteration.

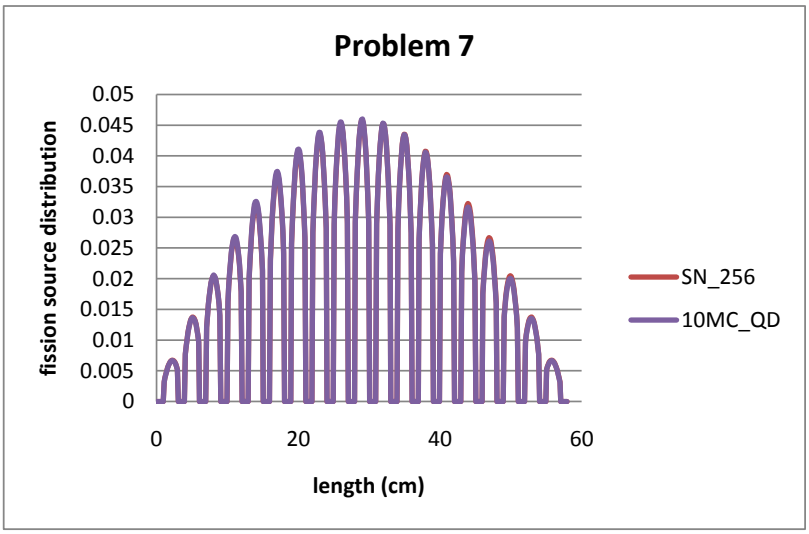

Figure 60: Problem 7: Fission distribution with 4,640,000 histories per MC generation and 10 MC generation/QD iteration.

The fission source distribution for the calculations for Problem 8a are shown in Figures 65 through 68, the convergence of the the k-eigenvalue are shown in Figures 69 through 70, and the slowest converging Eddington factor shown in Figures 71 through 72.

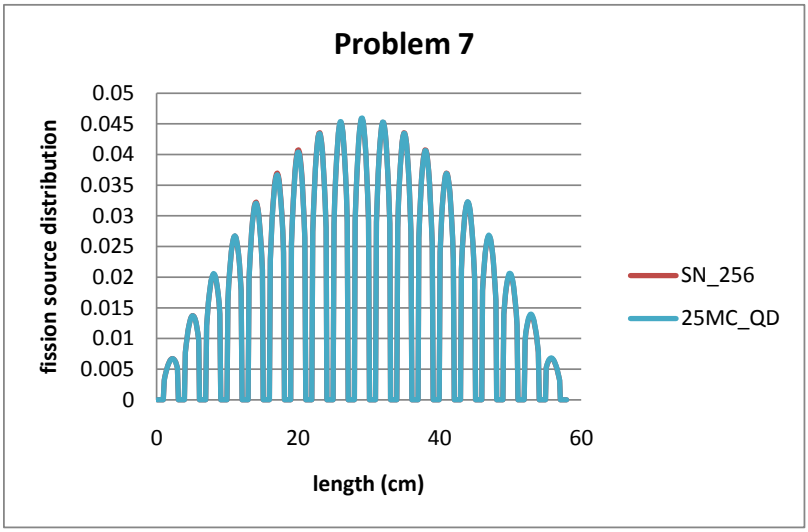

Figure 61: Problem 7: Fission distribution with 4,640,000 histories per MC generation and 25 MC generation/QD iteration.

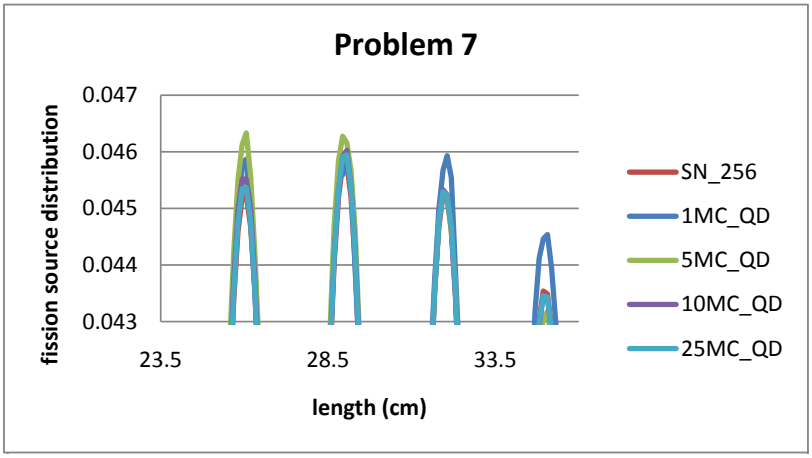

Figure 62: Problem 7: Fission distribution with 4,640,000 histories per MC generation in the middle of the slab.

As was seen in previous problems, the convergence of the fission source distribution is a direct function of the number of histories per generation used in the MC to solve for the Eddington factors. This can be accomplished by increasing the number of histories per MC generation or by increasing the number of MC generations per QD solve.

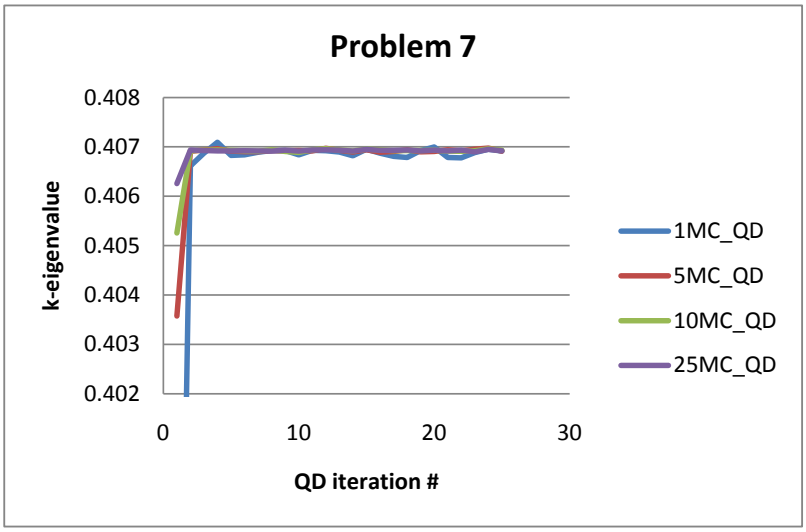

Figure 63: Problem 7: Convergence of k-eigenvalue with 4,640,000 histories per MC generation.

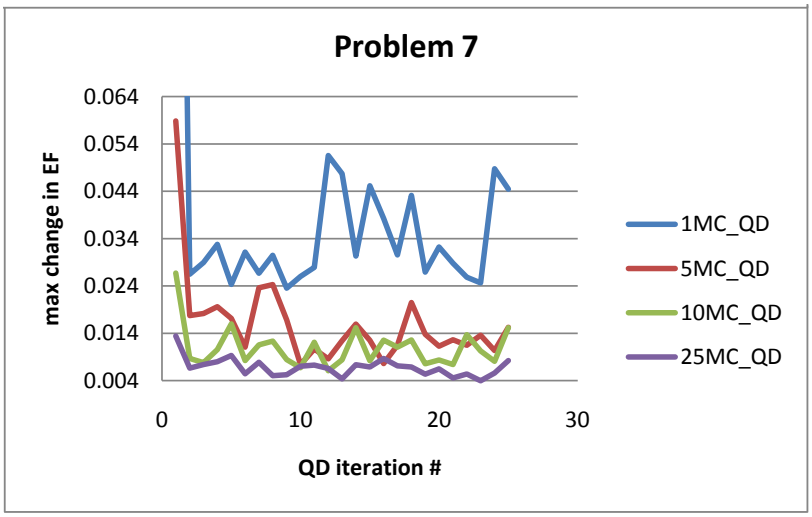

Figure 64: Problem 7: Convergence of Eddington factors with 4,640,000 histories per MC generation.

Figures 69 through 70 show that the k-eigenvalue converges for Problem 8a after only a couple iterations. However, as shown in Table 15 a more accurate and precise k-eigenvalue can be obtained by averaging the k-eigenvalues from all QD iterations. In all calculations performed a total of 25 MC/QD iterations were

Pr. 7	4,640,000
1	0.406224±0.00326
5	0.406790±0.000670
10	0.406861±0.000335
25	0.406899±0.000135

Table 13: k-eigenvalue (Problem 7); particles per generation vs. number of MC runs averaged per QD solve. Each k-eigenvalue is an average of the eigenvalues from 25 QD iterations.

Pr. 7b	4,640,000
1	0.405836±0.00330
5	0.406356±0.000686
10	0.406434±0.000345
25	0.406475±0.000136

Table 14: k-eigenvalue (Problem 7b); particles per generation vs. number of MC runs averaged per QD solve. Each k-eigenvalue is an average of the eigenvalues from 25 QD iterations.

done. A more precise k-eigenvalue could be obtained by increasing the number of QD iterations and averaging the eigenvalues from all iterations. The k-eigenvalue obtained for Problem 8a from the simple corner balance method using the S_{256} Gauss-Legendre quadrature set was 0.21259. Although the S_{256} value falls within one standard deviation of many of k-eigenvalues for the calculations performed on Problem 8a listed in Table 15 most of the averaged QD eigenvalues are high in the fourth significant figure with a difference of reactivity of approximately \$1.00. Results from Problem 9, show that this difference is a result of the spatial discretization.

Figures 71 through 72 show the slowest converging Eddington factor for each calculation of Problem 8a. The accuracy of the Eddington Factors is a function of the total number of histories used in the MC solver. The total number of histories

can be increased by either increasing the number of histories per generation or by increasing the number of MC generations per QD solve.

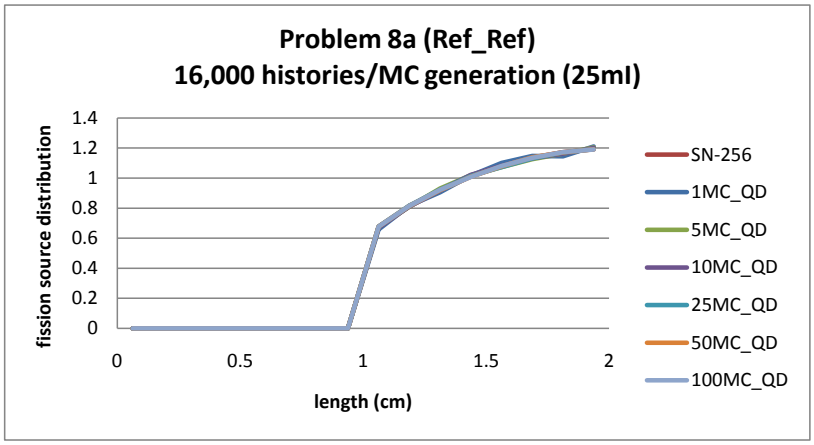

Figure 65: Problem 8a: Fission distribution with 16,000 histories per MC generation.

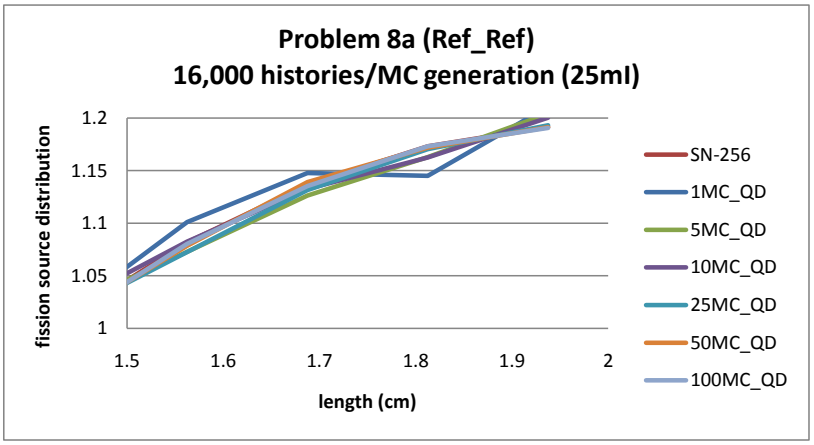

Figure 66: Problem 8a: Fission distribution with 16,000 histories per MC generation at right edge.

The fission source distribution for the calculations for Problem 8b are shown in Figures 73 through 76, the convergence of the the k-eigenvalue are shown in Figures 77 and 78, and the slowest converging Eddington factor shown in Figures 79 and 80.

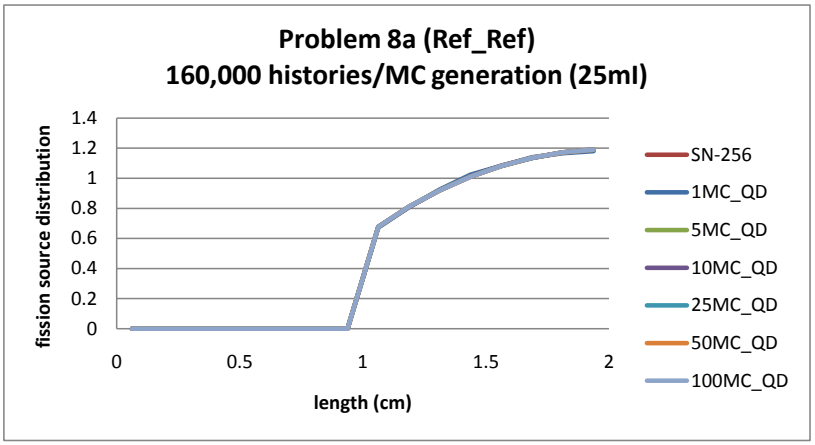

Figure 67: Problem 8a: Fission distribution with 160,000 histories per MC generation.

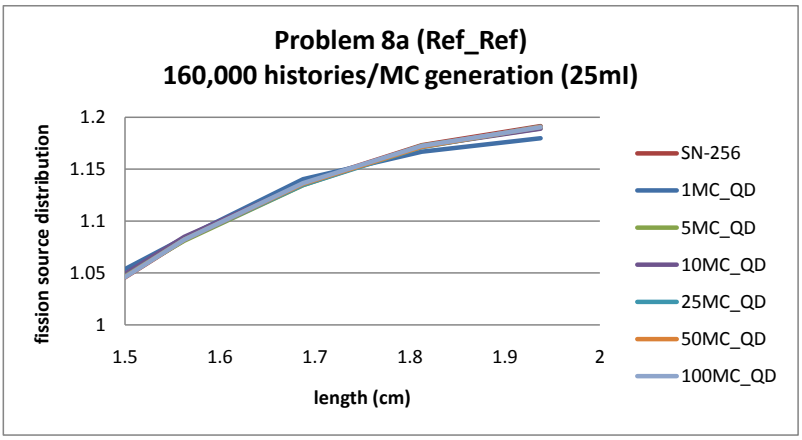

Figure 68: Problem 8a: Fission distribution with 160,000 histories per MC generation at right edge.

As was seen in previous problems, the convergence of the fission source distribution is a direct function of the number of histories per generation used in the MC to solve for the Eddington factors. This can be accomplished by increasing the number of histories per MC generation or by increasing the number of MC generations per QD solve.

Figures 77 and 78 show that the k-eigenvalue converges for Problem 8b after only a couple iterations. However, as shown in Table 16 a more accurate and

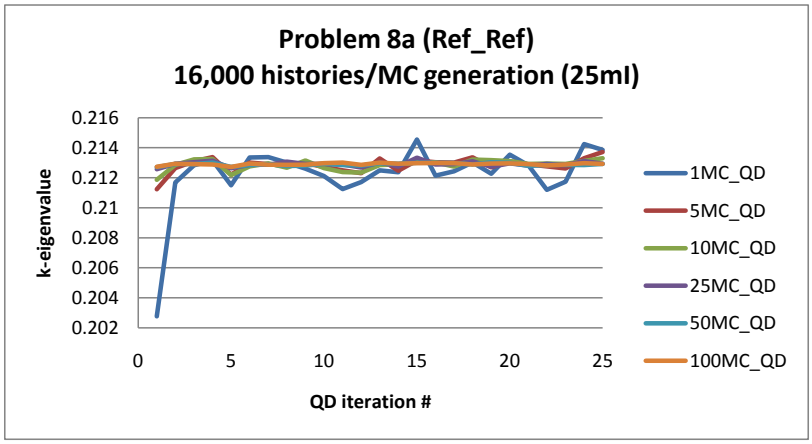

Figure 69: Problem 8a: Convergence of k-eigenvalue with 16,000 histories per MC generation.

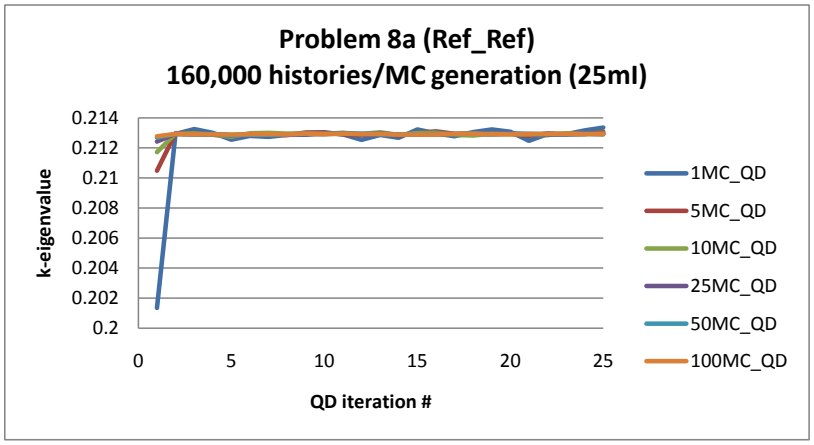

Figure 70: Problem 8a: Convergence of k-eigenvalue with 160,000 histories per MC generation.

precise k-eigenvalue can be obtained by averaging the k-eigenvalues from all QD iterations. In all calculations performed a total of 25 MC/QD iterations were done. As discussed above a more precise k-eigenvalue could be obtained by increasing the number of QD iterations and averaging the eigenvalues from all iterations. The k-eigenvalue obtained for Problem 8b from the simple corner balance method using the S_{256} Guass-Legendre quadrature set was 0.20515. Table 16 shows that the averaged MC/QD eigenvalues are high in the fourth significant figure with a

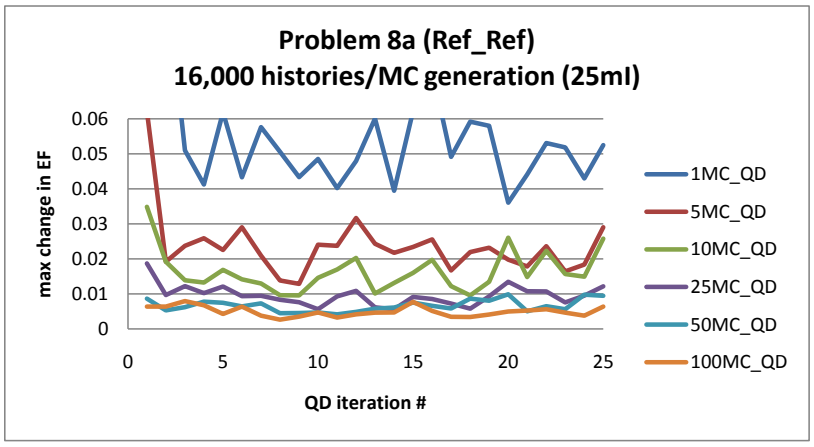

Figure 71: Problem 8a: Convergence of Eddington factors with 16,000 histories per MC generation.

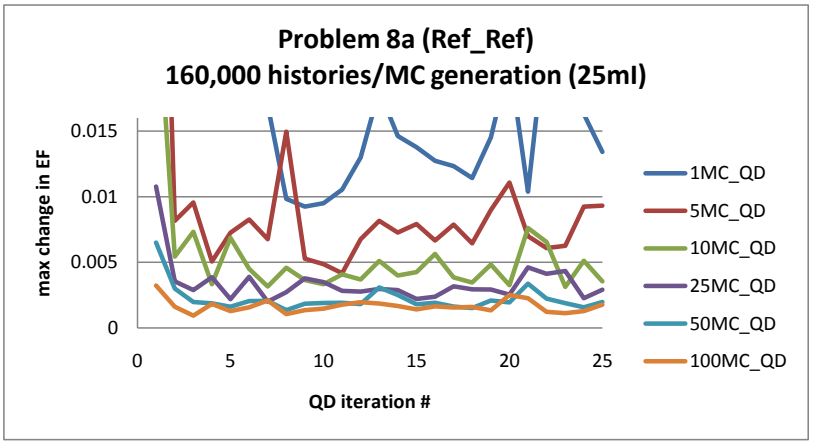

Figure 72: Problem 8a: Convergence of Eddington factors with 160,000 histories per MC generation.

difference of reactivity of approximately \$1.00. Results from Problem 9b, show that this difference is a result of the spatial discretization.

Figures 79 and 80 show the slowest converging Eddington factor for each calculation performed for Problem 8b. Figures 79 and 80 show that the accuracy of the Eddington factors is a function of the total number of histories used in the MC solver. The total number of histories can be increased by either increasing the number of histories per generation or by increasing the number of MC generations

Pr. 8a	16,000	160,000	1,600,000
1	0.212241±0.00217	0.212457±0.00233	N/A
5	0.212845±0.000490	0.212833±0.000497	N/A
10	0.212859±0.000357	0.212883±0.000254	N/A
25	0.212912±0.000169	0.212892±0.000104	N/A
50	0.212891±0.000091	0.212905±0.000052	N/A
100	0.212909±0.000073	0.212909±0.000035	0.212904±0.000025

Table 15: k-eigenvalue (Problem 8a); particles per generation vs. number of MC runs averaged per QD solve. Each k-eigenvalue is an average of the eigenvalues from 25 QD iterations.

per QD solve.

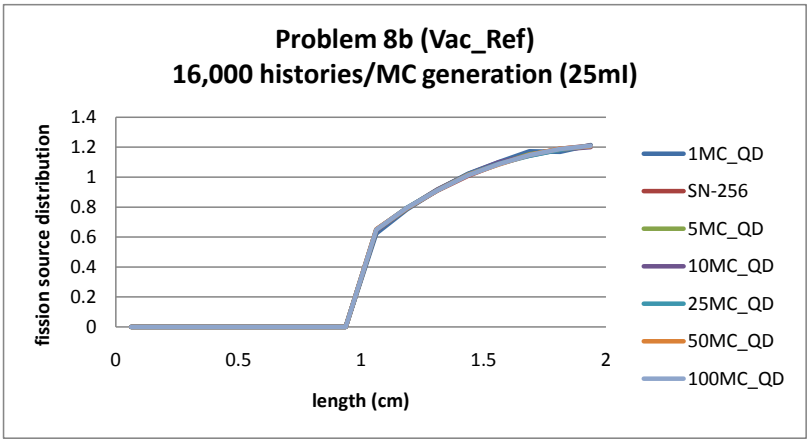

Figure 73: Problem 8b: Fission distribution with 16,000 histories per MC generation.

3.3.8 Test Problems #9a and 9b

Results for Problem 9a (Problem 9 with both boundaries reflecting) are shown in Table 17. We have performed calculations of this problem with 16000 and 160000 histories per generation, and choices of 1, 5, 10, 25, 50, and 100 Monte Carlo generations per QD solve.

Results for Problem 9b (Problem 9 with left boundary vacuum/right boundary

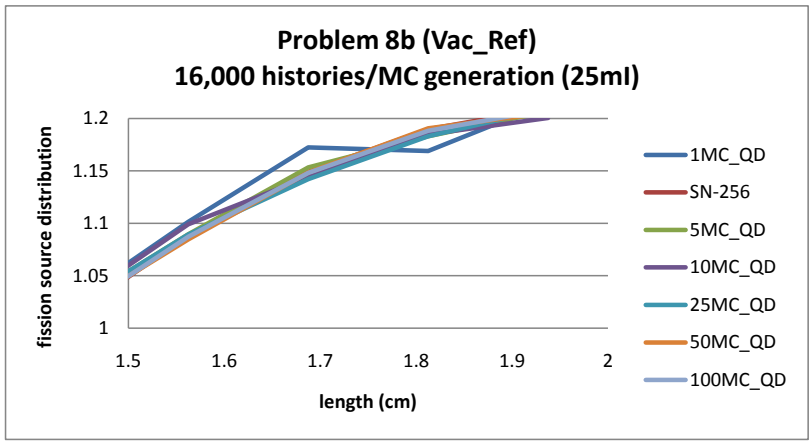

Figure 74: Problem 8b: Fission distribution with 16,000 histories per MC generation at right edge.

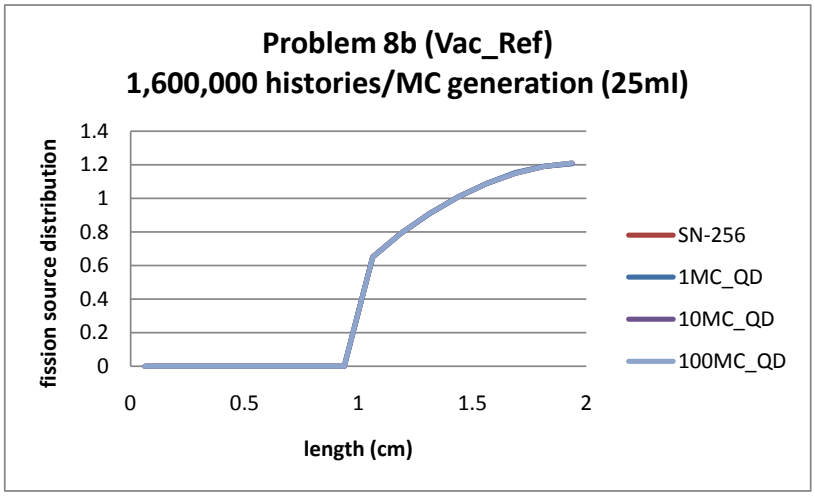

Figure 75: Problem 8b: Fission distribution with 1,600,000 histories per MC generation.

reflecting) are shown in Table 18. We have performed calculations of this problem with 16000, 160000, and 1,600,000 histories per generation, and choices of 1, 5, 10, 25, 50, and 100 Monte Carlo generations per QD solve.

The k-eigenvalue result for Problem 9a using the S_{256} Guass-Legendre quadrature set and simple corner balance discretization was 0.21259 which falls within one standard deviation of all the MC/QD hybrid results for Problem 9a listed in

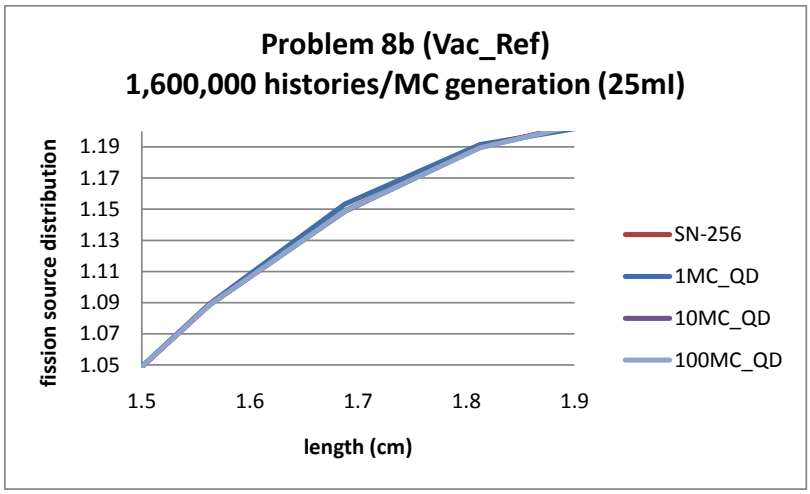

Figure 76: Problem 8b: Fission distribution with 1,600,000 histories per MC generation at right edge.

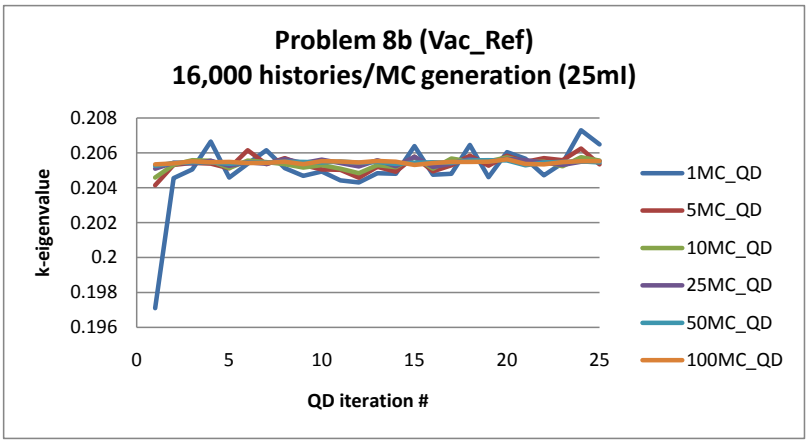

Figure 77: Problem 8b: Convergence of k-eigenvalue with 16,000 histories per MC generation.

Table 17. Comparing the k-eigenvalues from Problem 9a with Problem 8a show that increased spatial resolution significantly increased the accuracy of the MC/QD hybrid method.

Similarly, for Problem 9b the k-eigenvalue obtained using the S_{256} Gauss-Legendre quadrature set and simple corner balance discretization was 0.20515 which falls within one standard deviation of all the MC/QD hybrid results for

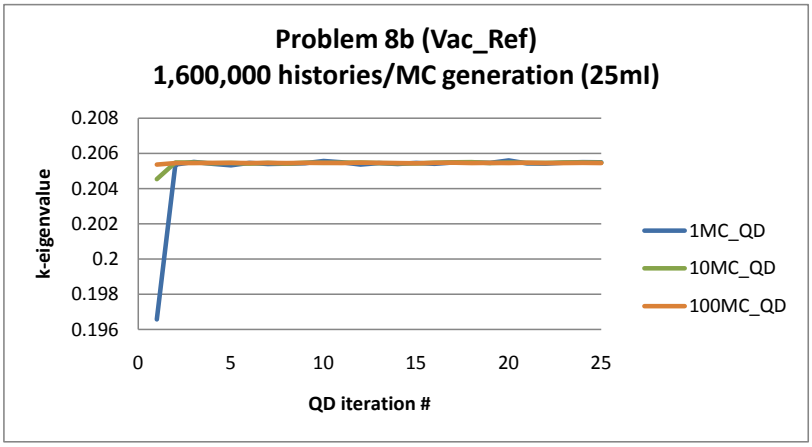

Figure 78: Problem 8b: Convergence of k-eigenvalue with 1,600,000 histories per MC generation.

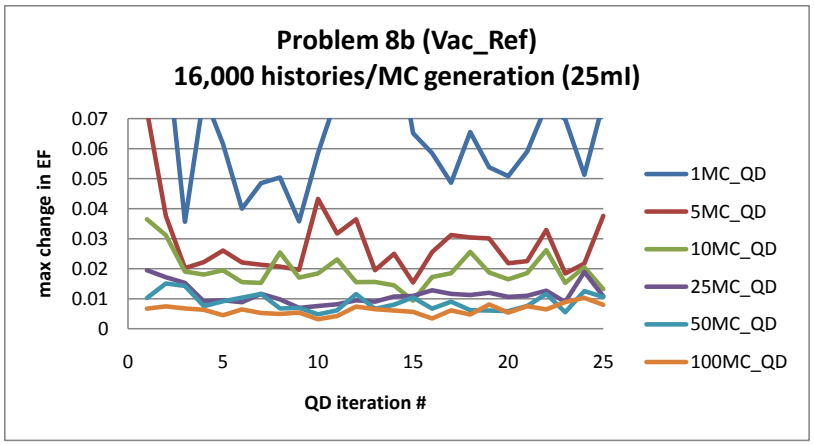

Figure 79: Problem 8b: Convergence of Eddington factors with 16,000 histories per MC generation.

Problem 9b listed in Table 18. Again, comparing the k-eigenvalues from Problem 9b with those from Problem 8b it can be seen that the increased spacial resolution in Problem 9 significantly increased the accuracy of the MC/QD hybrid method.

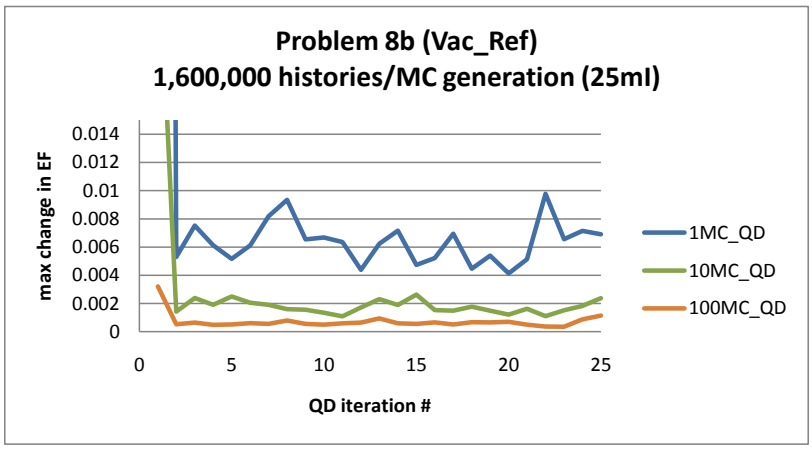

Figure 80: Problem 8b: Convergence of Eddington factors with 1,600,000 histories per MC generation.

Pr. 8b	**16,000**	**160,000**	**1,600,000**
1	0.205005±0.00184	0.205088±0.00180	0.205095±0.00178
5	0.205356±0.000463	0.205350±0.000370	N/A
10	0.205365±0.000288	0.205428±0.000213	0.205427±0.000186
25	0.205444±0.000167	0.205440±0.000094	N/A
50	0.205449±0.000076	0.205442±0.000051	N/A
100	0.205455±0.000076	0.205454±0.000031	0.205453±0.000019

Table 16: k-eigenvalue (Problem 8b); particles per generation vs. number of MC runs averaged per QD solve. Each k-eigenvalue is an average of the eigenvalues from 25 QD iterations.

Pr. 9a	**16,000**	**160,000**
1	0.212152±0.00266	0.212176±0.00231
5	0.212585±0.000700	0.212520±0.000474
10	0.212580±0.000348	0.212544±0.000254
25	0.212644±0.000212	0.212566±0.000123
50	0.212577±0.000131	0.212598±0.000068
100	0.212563±0.000092	0.212596±0.000038

Table 17: k-eigenvalue (Problem 9a); particles per generation vs. number of MC runs averaged per QD solve. Each k-eigenvalue is an average of the eigenvalues from 25 QD iterations.

Pr. 9b	**16,000**	**160,000**	**1,600,000**
1	0.204725±0.00215	0.204811±0.00186	0.204774±0.00179
5	0.205163±0.000623	0.205071±0.000410	N/A
10	0.205147±0.000308	0.205104±0.000208	0.205122±0.000186
25	0.205148±0.000154	0.205135±0.000101	N/A
50	0.205127±0.000093	0.205153±0.000046	N/A
100	0.205120±0.000066	0.205154±0.000028	0.205161±0.000018

Table 18: k-eigenvalue (Problem 9b); particles per generation vs. number of MC runs averaged per QD solve. Each k-eigenvalue is an average of the eigenvalues from 25 QD iterations.

4 Conclusions

4.1 Introduction

This chapter will discuss the results presented in Section 3. This includes an analysis of the results of the mono-energetic and multigroup hybrid Quasi-diffusion/Monte Carlo method compared to analog Monte Carlo and S_N Gauss Legendre quadrature set with simple corner balance discretization. The accuracy and precision of the Quasi-diffusion/Monte Carlo method will all be discussed based on material properties, discretization, and required computational power and the reasons for trends seen will be explained. This section will end with some ideas for future work.

4.2 Conclusions and Future Work

The hybrid MC/QD method was shown to accurately and precisely predict the k-eigenvalue and fission source distribution for 9 different test problems, many of which had significant spacial gradients and large dominance ratios. For the simple test problems it was clear that the MC/QD method was much more efficient. However, as was shown in the problems with multiple energy groups, increased spatial resolution was necessary to obtain the accuracy desired. Depending upon the difficulty of the problem and the necessary spatial resolution required, the MC/QD hybrid method performs with varying degrees of efficiently. As the spatial resolution was increased, more computational work was required in the Monte Carlo code to calculate the Eddington Factors and this significantly increase the computational time.

The accuracy of the Eddington factors, and subsequently the accuracy of the k-eigenvalue and fission distribution, was found to be directly proportional to the number of histories performed during the MC solve. Increasing the number of histories per generation or increasing the total number of generations per MC solve were equally effective.

The k-eigenvalue converged rapidly (generally within a couple MC/QD generations). However, the precision of the k-eigenvalue was greatly increased by averaging many generations.

Finite volume discretization was used in the LOQD solver. Future work using other discretization methods that have a higher order of accuracy, like simple corner balance, would be of value. With a higher order discretization scheme it may be possible to decrease the spatial resolution in the LOQD solver and thus decrease the computational time required.

There needs to be more work done to determine quantitatively the total computational power required in order to compare more effectively the MC/QD hybrid method with standard Monte Carlo. An addition to the program that would make the quantification much easier would be a subroutine that has an algorithm for splitting the regions into increasing numbers of cells until a spatial resolution is reached such that the k-eigenvalue does not significantly change with increased spatial resolution. In addition, it would be interesting to see if the spatial resolution required is effected by the number of energy groups in a problem.

Future work that would also be of value would be to investigate how the MC/QD hybrid method performs in two or three dimensional problems.

Bibliography

[Ada. nd] Adams, Marvin. L., Larsen, Edward W., "Fast Iterative Methods for Discrete-ordinates Particle Transport Calculations" *Progress in Nuclear Energy* **40(1)**, 3-159 (2002).

[Aks. 1979] Aksenov, N.N., Gol'din, V.Ya., "Computation of the Two-Dimensional Stationary Equation of neutron Transfer by the Quasi-Diffusion Method" *U.S.S.R. Computational Mathematics and Mathematical Physics* **19**, 263-266 (1979)

[Ani. 1993] Anistratov, Dmitri Yu., Gol'din, Vladimir Ya., "Nonlinear Methods for Solving Particle Transport Problems" *Transport Theory and Statistical Physics*, **22(2&3)**, 125-163 (1993).

[Ani. 2005] Anistratov, Dmitri Y., "Consistant Spatial Approximation of the Low-Order Quasi-Diffusion Equations on Coarse Grids" *Nuclear Science and Engineering*, **149**, 138-161 (2005).

[Ari. 2000] Aristova, E.N., Gol'din, V.Ya, "Computation of Anisotropy Scattering of Solar Radiation in Atmosphere (Monoenergetic Case)" *Journal of Quantitative Spectroscopy and Radiative Transfer* **67**, 139-157 (2000).

[Cef. 1990] Cefus, G.R., Larsen, E.W., "Stability Analysis of the Quasidiffusion and Second Moments Methods for Iteratively Solving Discrete-Ordinates Problems" *Transport Theory and Statistical Physics* **18(5-6)**, 493-511 (1990).

[Dud. 1976] Duderstadt, J.J., Hamilton, L.J., **Nuclear Reactor Analysis** John Wiley & Sons, Inc.,(1976).

[Gol. 1964] Gol'din, V.Ya., "A Quasi-Diffusion Method for Solving the Kinetic Equation", *Zh. Vych. Mat. I Mat. Fiz.* **4(1078)**, (1964). English translation published. *U.S.S.R. Computational Mathematics and Mathematical Physics*, **4(6)**, 136-149 (1967).

[Gol. 1972] Gol'din, V.Ya., Chetverushkin, B.N., "Methods of Solving One-Dimensional Problems of Radiation Gas Dynamics" *U.S.S.R. computational Mathematics and Mathematical Physics* **4(12)**, 177-189 (1972).

[Hag. 2003] Haghighat, A., Wagner, J.C., "Monte Carlo Variance Reduction with Deterministic Importance Functions" *Progress in Nuclear Energy* **42**, 25 (2003).

[Hik. 2005] Hikaru, H., Anistratov, D.Y., Adams, M.L., "Splitting Method for Solving the Coarse-Mesh Discretized Low-Order Quasi-Diffusion Equations" *Nuclear Science and Engineering* **149**, 162-181 (2005)

[Lar. 2007] Larsen, E.W., Yang, J., "New 'Monte Carlo Functional' Methods for Estimating k-Eigenvalues and Eigenfunctions" *(*Trans. American Nuclear Society **97**, 469 (2007)

[Lar. 2008] Larsen, E.W., Yang, J., "A 'Functional Monte Carlo' Method for k-Eigenvalue Problems" *(*Nuclear Science and Engineering **159**, 107 (2008)

[Lew. 1993] Lewis, E.E., Miller, Jr., W.F., **Computational Methods of Neutron Transport** American Nuclear Society, Inc., La Grange Park, IL (1993)

[MCNP 2009] *http://www-rsicc.ornl.gov/*

[Met. 1987] Metropolis, N., "The Beginning of the Monte Carlo Method" *Los Alamos Science*, **Special Issue**,(1987).

[Mif. 1993] Miften, M.M., Larsen, Edward W., "The Quasi-Diffusion Method for Solving Transport Problems in Planar and Spherical Geometries" *Transport Theory and Statistical Physics*, **22(2&3)**, 165-186 (1993).

[Smi. 2005] Smith, H.P., Wagner, J.C., "A Case Study in Manual and Automated Monte Carlo Variance Reduction with a Deep Penetration Reactor Shielding Problem" *Nuclear Science and Engineering*, **149**, 23 (2005).

[Tro. 1968] Troshchiev, V.E., Yudintsev, V.F., Fedyanin, V.I., "Acceleration of the Convergence of Iterations in Solving the Kinetic Equation" *U.S.S.R. Computational Mathematics and mathematical Physics*, **8**, 298-308 (1968).

[Urb. 1995] Urbatsch, Todd J., "Iterative Acceleration Methods for Monte Carlo and Deterministic Criticality Calculations" **Todd Urbatsch's PhD thesis** University of Michigan, Ann Arbor, MI (1995).

[Wag. 2010] Wagner, J.C., Mosher, S.W. "Forward-Weighted CADIS Method for Variance Reduction of Monte Carlo Reactor Analysis" *Trans. American Nuclear Society*, **mtg**, Winter (2010).